The Astrophysical Journal, 674:909–926, 2008 February 20

VLT SPECTROSCOPY OF GLOBULAR CLUSTERS IN LOW SURFACE BRIGHTNESS DWARF GALAXIES[1]

Thomas H. Puzia[2,3] and Margarita E. Sharina[4,5]

Received 2007 August 16; accepted 2007 October 5

ABSTRACT

We present VLT/FORS2 spectroscopic observations of globular clusters (GCs) in five low surface brightness dwarf galaxies: KK 211 and KK 221, both dwarf spheroidal satellites (dSph) of NGC 5128; dSph KK 84 located close to the isolated S0 galaxy NGC 3115; and two isolated dwarf irregular (dIrr) galaxies, UGC 3755 and ESO 490−17. Our sample is selected from the Sharina et al. database of *HST* WFPC2 photometry of GC candidates in dwarf galaxies. For objects with accurate radial velocity measurements we confirm 26 as genuine GCs out of the 27 selected candidates from our WFPC2 survey. One candidate appears to be a distant galaxy. Our measurements of the Lick absorption-line indices in the spectra of confirmed GCs and the subsequent comparison with SSP model predictions show that all confirmed GCs in dSphs are old, except GC KK 211−3−149 (6 ± 2 Gyr), which we consider to be the nucleus of KK 211. GCs in UGC 3755 and ESO 490−17 show a spread in ages ranging from $t > 10$ Gyr to around 1 Gyr. Most of our sample GCs have low metallicities $[Z/\mathrm{H}] \leq -1$. Two relatively metal-rich clusters with $[Z/\mathrm{H}] \approx -0.3$ are likely to be associated with NGC 3115. Our sample GCs show in general a complex distribution of α-element enhancement with a mean $\langle[\alpha/\mathrm{Fe}]\rangle = 0.19 \pm 0.04$ derived with the χ^2 minimization technique and 0.18 ± 0.12 dex computed with the iterative approach. These values are slightly lower than the mean $\langle[\alpha/\mathrm{Fe}]\rangle = 0.29 \pm 0.01$ for typical Milky Way GCs. We compare other abundance ratios with those of Local Group GCs and find indications for systematic differences in N and Ca abundance. The specific frequencies, S_N, of our sample galaxies are in line with the predictions of a simple mass-loss model for dwarf galaxies and compare well with S_N values found for dwarf galaxies in nearby galaxy clusters.

Subject headings: galaxies: dwarf — galaxies: star clusters — globular clusters: general

1. INTRODUCTION

The hierarchical structure formation scenario predicts that dwarf galaxies are the first systems to form in the universe (Peebles & Dicke 1968), and that more massive galaxies form through dissipative processes from these smaller subunits. The involved physical mechanisms of this sequence depend on the density and mass of the parent dark matter halo, in the sense that more massive halos initiate star formation at earlier epochs and form their stars at a faster rate (e.g., Peebles 2002; Renzini 2006; Ellis 2007). Because of this environmental gradient, we expect that dwarf galaxies in the field formed the first stellar population relatively late and at a lower pace compared to their counterparts in dense galaxy clusters. In other words, the difference in age and chemical composition between the oldest stellar populations in cluster and field dwarf galaxies should reflect the delay in the onset of structure formation in these two environments.

The task of measuring the age and chemical composition of the oldest stellar populations in distant dwarf galaxies from their integrated light is very challenging. An alternative approach is to investigate the oldest globular clusters (GCs) that are found in dwarf galaxies. Several photometric surveys of extragalactic GCs in dwarf galaxies outside the Local Group have been performed in the past decade (see review by Miller 2006). However, only a handful of those were followed up with 8–10 m class telescopes to derive spectroscopic ages and chemical composition. Observations of galaxies in groups and clusters provide more and more evidence that environment is a major factor influencing the process of GC formation (e.g., West 1993; Tully et al. 2002; Grebel & Harbeck 2003; Miller et al. 1998). Recent progress in modeling the assembly history of GC systems in massive elliptical galaxies suggests that a significant fraction of metal-poor GCs were accreted from dwarf satellites at later times compared to the number of GCs initially formed in the parent galaxy halo (Pipino et al. 2007). These results underline the ideas put forward in the work of Forte et al. (1982) and Muzzio (1987), as well as the models of Côté et al. (1998, 2002); Hilker et al. (1999), who suggested that the rich GC systems of massive galaxies may be the result of significant GC accretion through tidal stripping of less massive systems.

Spectroscopic studies of a few GCs in cluster and field dwarf galaxies showed that most of these systems host at least some old GCs with ages $t \gtrsim 10$ Gyr (Puzia et al. 2000; Sharina et al. 2003; Strader et al. 2003a, 2003b; Beasley et al. 2006; Conselice 2006). Although today's accuracy of relative spectroscopic age determinations ($\Delta t/t \approx 0.2$–0.3) is not sufficient to resolve the expected delay of $\sim$0.5–4 Gyr in the onset of star formation between cluster and field environment; depending on cosmology, ionizing source population, ionization feedback efficiency, etc. (see Kauffmann 1996; Treu et al. 2005; Thomas et al. 2005; De Lucia et al. 2006; Clemens et al. 2006), the old ages combined with information on abundance ratios can provide a powerful tool to decide whether stellar populations in field dwarf galaxies followed the same early enrichment history as their analogs in denser environments. Furthermore, any difference in GC chemical composition between dwarf and more massive galaxies opens an attractive way of chemically tagging accreted subpopulations in massive halos and, therefore, enables us to quantify the mass accretion history of galaxies, a task that for old galaxies is infeasible from studies of the diffuse galaxy light alone. Similar ideas have been formulated

[1] Based on observations made with ESO Telescopes at the Paranal Observatory under program ID P76.AB-0137.

[2] Herzberg Institute of Astrophysics, 5071 West Saanich Road, Victoria, BC V9E 2E7, Canada.

[3] Plaskett Fellow.

[4] Special Astrophysical Observatory, Russian Academy of Sciences, N.Arkhyz, KChR, 369167, Russia.

[5] Isaac Newton Institute of Chile, SAO Branch.

TABLE 1
PROPERTIES OF SAMPLE DWARF GALAXIES

Galaxy (1)	R.A. (J2000.0) (2)	Decl. (J2000.0) (3)	μ_0 (4)	D_{MD} (5)	A_B (6)	B (7)	$B-I$ (8)	M_V (9)	N_{GC} (10)	S_N (11)
KK 211, AM1339-445	13 42 06	−45 13 18	27.77	0.25	0.477	16.3 ± 0.2	1.8 ± 0.2	−12.58	2	18.6
KK 221	13 48 46	−46 59 49	28.00	0.50	0.596	17.3 ± 0.4	2.0 ± 0.4	−11.96	6	95.1
KK 084, UA 200, KD G65	10 05 34	−07 44 57	29.93	0.03	0.205	16.4 ± 0.2	1.7 ± 0.2	−14.40	7	10.4
UGC 3755, PGC 020445	07 13 52	+10 31 19	29.35	∼5	0.384	14.1 ± 0.2	1.1 ± 0.2	−16.12	32	11.4
E490−017, PGC 019337	06 37 57	−25 59 59	28.13	4.50	0.377	14.1 ± 0.2	1.1 ± 0.2	−14.90	5	5.4

NOTES.—Columns contain the following data: (1) galaxy name; (2) and (3) equatorial coordinates; (4) and (5) are the distance modulus and distance from the nearest bright galaxy in Mpc from Karachentsev et al. (2004) and from Tully et al. (2006) for UGC 3755; (6) reddening from Schlegel et al. (1998) in the B band; (7) and (8) the integrated B magnitude and the integrated $B-I$ color, derived from surface photometry on the VLT-FORS2 images in this work (see Appendix A); (9) absolute V magnitude from SPM05; (10) number of GCs according to SPM05 and this paper; (11) specific frequency, $S_N = N_{GC}10^{0.4(M_V+15)}$ (Harris & van den Bergh 1981). Units of right ascension are hours, minutes, and seconds, and units of declination are degrees, arcminutes, and arcseconds.

for stellar populations that make up the diffuse component of the most nearby galaxies, which are close enough for high-resolution spectroscopy of individual stars (Freeman & Bland-Hawthorn 2002; Geisler et al. 2007). The obvious advantage of GC systems is that their spectra can be observed out to about 10 times greater distances.

In this work we analyze spectroscopic observations of GCs in dwarf irregular (dIrr) and dwarf spheroidal galaxies (dSph) in the field/group environment. Our sample consists of systems that are representatives of the lowest mass bin of the Local Volume (LV) galaxy population, limited to distances $D < 10$ Mpc. We refer to Karachentseva et al. (1985) and Grebel (1999) for a morphological type definition of our sample galaxies. The paper is organized as follows. In § 2 we describe our observations and data reduction, as well as the methods of measuring radial velocities. Section 3 summarizes the measurement of Lick line indices, their calibration, and the determination of spectroscopic ages, metallicities, and abundance ratios. Section 4 is devoted to the discussion of our results. Conclusions are presented in § 5.

2. OBSERVATIONS

2.1. *Sample Selection*

All target galaxies are part of the Sharina et al. (2005, hereafter SPM05) sample for which detailed information on luminosities, colors, and structural parameters of GC candidates is available from HST data. The targets were selected based on the number of GC candidates and the optimization of the observing strategy at the time of scheduled observations. The main characteristics of our sample galaxies are presented in Table 1. KK 211 and KK 221 are two of the faintest dSph galaxies in the Centaurus A group. The dSph galaxy KK 84 is the nearest satellite of the giant field S0 galaxy NGC 3115. UGC 3755,[6] which hosts one of the richest GC system among isolated dwarf galaxies (see Table 1), and ESO 490−17 are both highly isolated dIrrs. In general, the specific frequencies are high for all our sample galaxies. It will be shown in the last section, that these S_N values correspond to the predictions of galaxy evolution models that include significant mass loss, which strongly affects the star formation processes in low-mass galaxies.

Detailed CMD studies of the Local Group dwarf galaxies show that each low-mass galaxy has its own complex star formation history (SFH) (e.g., Grebel & Harbeck 2003). However, in contrast to dIrrs, dSphs are composed mainly of old and intermediate-age stars, and do not contain young stellar populations (e.g., Holtzman et al. 2006). We will test whether this difference is reflected in the GC populations of our sample field/group dwarfs and investigate the chemical compositions of their GC stellar populations.

2.2. *Preimaging Data*

All preimaging data were obtained with the FORS2 instrument at UT1 (unit telescope 1, ANTU) as par of the program 76.B-0137. A journal of the preimaging observations is provided in Table 2. All images were reduced using standard techniques (bias subtraction and flat fielding). We used the FIMS (FORS Instrumental masks simulator) task `fsmosaic` to merge two files of each image. To register and combine the six subintegrations obtained in each filter we used the tasks `ccmap` and `imcombine` in IRAF.[7] Aperture photometry of GC candidates (GCCs) was performed using the PHOT task of DAOPHOT-II (Stetson 1987) package implemented in MIDAS. The detection threshold was set to 3 σ above the background. The minimum FWHM input parameter was $\sim 0.76''$, corresponding to a typical stellar FWHM. To convert instrumental magnitudes into the Johnson-Cousins standard system we applied the FORS2 photometric zero points[8]: $B_0 = 27.356 \pm 0.007$ (for chip 1), $B_0 = 27.338 \pm 0.005$ (for chip 2), $I_0 = 27.555 \pm 0.1$ (for chip 1), $I_0 = 27.559 \pm 0.07$ (for

[6] Strictly speaking UGC 3755 is a borderline low surface brightness galaxy according to the definition outlined by Impey & Bothun (1997): $\bar{\mu}_{0,B} \geq 22.5 - 23$ mag arcsec^{-2}.

[7] IRAF is distributed by the National Optical Astronomy Observatory, which operated by the Association of Universities for Research in Astronomy, Inc., under cooperative agreement with the National Science Foundation.

[8] See http://www.eso.org/observing/dfo/quality/FORS2/qc/zeropoints/zeropoints.html.

TABLE 2
JOURNAL OF PREIMAGING OBSERVATIONS

Object	Date	Filter	t_{exp} (s)	Seeing (arcsec)	Air Mass
KK 211	2005 Aug 25	B	6 × 180	1.0	1.740
	2005 Aug 25	I	6 × 90	1.0	1.834
KK 221	2005 Aug 25	B	6 × 180	1.1	1.914
	2005 Aug 25	I	6 × 90	1.2	1.997
UGC 3755	2005 Nov 1	B	6 × 180	0.9	1.258
	2005 Nov 1	I	6 × 90	0.9	1.242
E490−017	2005 Nov 28	B	6 × 180	0.7	1.041
	2005 Nov 28	I	6 × 90	0.7	1.056
KK 084	2005 Dec 12	B	6 × 215	1.2	1.164
	2005 Dec 12	I	6 × 120	1.2	1.164

NOTE.—The exposure time is given in seconds.

chip 2), obtained from data taken during the same nights. Atmospheric extinction coefficients[9] were taken for 2006−01−01, $k_B = 0.269 \pm 0.016$ (for chip 1), $k_B = 0.22 \pm 0.22$ (for chip 2), $k_I = 0.150 \pm 0.018$ (for chip 1), $k_I = 0.135 \pm 0.015$ (for chip 2). Finally, the magnitudes of all GCCs were corrected for Galactic extinction using reddening maps from Schlegel et al. (1998). The accuracy of our photometry depends primarily on the accuracy of the background estimates. The uncertainties grow in the central regions of galaxies where the background is less homogeneous, and the images become increasingly affected by stellar crowding. In general, the errors of B and I magnitudes are less than 0.1 mag for objects brighter than 21.5 mag. The budget of errors includes the errors of aperture photometry, and the uncertainties of transformations into the standard B and I system. We consider the internal reddening within our sample galaxies to be $E_{(B-V)} \lesssim 0.1$ mag (James et al. 2005), given the similarity of these systems to nearby low surface brightness galaxies.

For our spectroscopic observations we selected GCCs with integrated colors $0.7 < (B-I)_0 < 2.3$, similar to the selection of Puzia et al. (2004, hereafter P04). In total we found 96, 74, 14, 19, and 11, objects in and around KK 084, UGC 3755, ESO 490−017, KK 221, and KK 211, respectively. The full list of GCCs detected on the VLT images with equatorial coordinates, B and I magnitudes, and spectroscopic classification of genuine GCs, foreground stars, and background galaxies is available on request from the authors (see also Tables 4 and 5). We point out that all GCCs that are listed in SPM05 are also included in the final target list and were all selected purely based on their $B-I$ colors.

To obtain accurate estimates of specific frequencies, we also perform surface photometry of our sample galaxies using the SURPHOT routine implemented in MIDAS. All steps are identical to those described in Makarova (1999). Table 1 documents the results, which are illustrated in Figure 9 and discussed in detail in Appendix A.

2.3. *Spectroscopic Data*

The spectroscopic data were obtained in the MXU mode with FORS2 using custom slit masks for KK 084, UGC 3755, ESO 490−017, KK 221, and KK 211 that contain 39, 39, 28, 36, and 26 objects in total, respectively. A journal of spectroscopic observations is provided in Table 3. The masks included our primary target GCCs, as well as mask-filler objects that were mostly stars and background galaxies. In general, due to the concentrated location of GCCs in the central regions of dwarf galaxies we primarily targeted GCCs from SPM05 and set slits on: all two GCCs in KK 211, all five GCCs in KK 221, three of five GCCs in ESO 490−017, 10 of 32 GCCs in UGC 3755, and seven of eight GCCs in KK 084 (KK 084−2−974 was not observed, see also Tables 4 and 5 for details).

The reduction of the spectroscopic data and the subsequent analysis were performed with a combination of MIDAS and IRAF tasks. After cosmic-ray removal and bias subtraction all frames were divided by a normalized flat-field image. For each slit a two-dimensional subsection of the CCD was extracted and then treated separately. To correct the effect of optical field distortions in the FORS field of view we applied the method described by P04, which is based on a two-dimensional wavelength solution assembled of one-dimensional solutions for each pixel row from arclamp spectra. For this task we used the LONG package in MIDAS. This procedure requires an accurate wavelength solution for each individual pixel row. To maximize the signal-to-noise ratio (S/N) of lines in the comparison arc spectrum we flat-fielded the arc spectrum to correct for small-scale fluctuations and applied a median filter to the frame using a rectangular filter window of one pixel in the dispersion direction and 3 pixels in the spatial direction. A typical accuracy of the two-dimensional dispersion solution was $\leq$0.2 Å. The extraction region was defined by tracing the GC spectrum along the wavelength dimension. The window width for the traced extraction was set so that the boundaries of spectra were at ∼15% of the peak flux in all cases, except for GCs 1182 and 2123 in UGC 3755, where the extraction window was set to a width of ∼20% of the peak flux, because of their location near regions of Hα emission.

To ensure that the dispersion solution was determined correctly we extracted the one-dimensional spectra using the method described above without subtracting the sky spectrum and determined the wavelengths of the telluric lines (Osterbrock et al. 1996, 2000). For few spectra we found systematic shifts of the order of $\lesssim$1 Å equal for all lines. Such shifts were corrected by adding of the corresponding correction term to the dispersion solution. The GC spectra (see Fig. 1) are then cross-correlated with spectra of radial-velocity standard stars observed in the same night using the `xcorrelate/image` procedure in MIDAS, which yields radial velocities according to the method of Tonry & Davis (1979). Table 5 summarizes the measured heliocentric radial velocities.

TABLE 3
JOURNAL OF SPECTROSCOPIC OBSERVATIONS

Object	Date	t_{exp}[a]	Seeing
E490−017	03.01.2006	4 × 1800	0.8
	04.01.2006	1800	1.6
KK 084	03.01.2006	5 × 1800	1.0
	04.01.2006	8 × 1800	1.5
	05.01.2006	4 × 1800	0.7
KK 221	03.01.2006	5 × 1800	1.0
UGC 3755	04.01.2006	6 × 1800	1.3
	05.01.2006	5 × 1800	0.8
KK 211	05.01.2006	5 × 1800	0.8
HD 013043	03.01.2006	4, 1	1.8
HR 0695	03.01.2006	2, 1	1.8
	04.01.2006	1, 1	1.8
HR 1506	03.01.2006	1, 8	1.8
	05.01.2006	1	0.8
HD 64606	04.01.2006	1, 3	1.8
HR 3905	04.01.2006	1, 5	1.8
HR 2233	05.01.2006	1, 1	1.3
HD 36003	05.01.2006	1, 2	1.3
HR 1015	05.01.2006	1, 3	1.3

[a] The exposure times for GCs (*upper part*) are given in multiples of seconds, while the exposure times for Lick standard stars are shown in seconds for each individual integration.

2.4. *Detection Efficiencies*

We present a resumé of GC detection efficiencies for our spectroscopic observations in Table 4. Numbers of detected GCCs within the FORS2 field of view with colors resembling those of GCCs, prepared masks for a part of them, confirmed genuine globular clusters, distant galaxies with radial velocities $\geq$1000 km s^{-1}, and Galactic stars with radial velocities ∼0 km s^{-1} are given for each galaxy, correspondingly. All observed GCCs from SPM05 appear to be genuine globular clusters, except a distant galaxy KK 084−4−967. Heliocentric radial velocities of spectroscopically confirmed GCs are similar to the system velocities of Cen A

[9] See http://www.eso.org/observing/dfo/quality/FORS2/qc/photcoeff/photcoeffs_fors2.html.

TABLE 4
Resumé of GC Detections

Name (1)	GCCs (2)	Objects Selected (3)	Number of Slits: Total (4)	Number of Slits: SPM05 (5)	GCs (6)	Galaxies (7)	Stars (8)	Faint Objects: Total (9)	Faint Objects: GCCs (10)
KK 211	2	11	26	2	2	5	12	7	
KK 221	5	19	36	5	6	6	5	19	KK 221−3−1062
KK 084	8	96	39	7	7	13	7	12	KK 84−2−789
UGC 3755	32	74	39	10	10	8	9	12	U3755−3−1963
E490−017	5	14	28	3	2	9	8	9	E490−017−3−1861

Notes.—Columns are as follows: (1) name; (2) number of GCCs in each galaxy listed by SPM05; (3) total number of GCCs selected on the VLT images; (4) slits on GCCs in total; (5) number of slits on SPM05 targets; (6) spectroscopically confirmed GCs; (7) number of background galaxies in slits; (8) Galactic stars; (9) faint object in total, the nature of which is unclear; (10) GCs that are too faint to measure their radial velocities with reliable accuracy from our observations.

and NGC 3115 in the cases of KK 211, KK 221, and KK 84, and to the velocities of the host galaxies measured using independent methods in the cases of UGC 3755 and E490−017 (Table 5). The radial velocity dispersion of the UGC 3755 sample is small $\sim$10 km s^{-1}, and the mean is consistent with the systemic value $V_h = 315$ km s^{-1} measured by Bicay & Giovanelli (1986). UGC 3755 is the only galaxy in our sample with a low enough systemic radial velocity so that a test of contamination likelihood by Galactic foreground stars is indicated. An evaluation of this likelihood with the stellar population synthesis models of the Milky Way (Robin et al. 2003) shows that the expected radial velocities of the thick disk, spheroid, and bulge component in the direction of UGC 3755 are significantly below 200 km s^{-1}. Combined with their diffuse (i.e., nonstellar) point-spread functions in the *Hubble Space Telescope* (*HST*) images and their color information all our GCCs in UGC 3755 with accurate radial velocity measurements (see Table 5) are highly unlikely to be foreground stars. We discovered three new GCs: KK 84−36n and KK 84−12n, and KK 221−12n (see Fig. 2). The equatorial coordinates, total B magnitudes, absolute B magnitudes, $B - V$, $B - I$ colors and radial velocities for all GCs confirmed or detected in this work are given in Table 5. In summary, our GCC selection efficiency based on the *HST* imaging survey presented in SPM05 is higher than 96% for the observed sample.

TABLE 5
Properties of Spectroscopically Confirmed GCs in our Sample LSB Dwarf Galaxies

GC (1)	R.A. (J2000.0) (2)	Decl. (J2000.0) (3)	B (4)	M_B (5)	$B - V$ (6)	$B - I$ (7)	V_h (8)
KK 211−3−149	13 42 05.6	−45 12 18	20.64	−7.13	0.69	1.51	580 ± 23
KK 211−3−917	13 42 08.0	−45 12 28	21.84	−5.93	0.93	1.64	620 ± 39
KK 221−2−608	13 48 55.1	−47 00 07	21.08	−6.92	1.12	1.85	541 ± 32
KK 221−2−883	13 48 53.0	−47 00 16	22.07	−5.93	1.14	1.89	546 ± 46
KK 221−2−966	13 48 50.5	−47 00 07	19.20	−8.80	1.00	1.78	509 ± 25
KK 221−2−1090	13 48 49.6	−47 00 11	21.20	−6.80	0.97	1.63	478 ± 29
KK 221−24n	13 48 43.6	−46 58 59	20.70	−7.30	...	1.63	512 ± 31
KK 221−27n	13 48 39.0	−46 59 49	22.26	−5.44	...	1.74	466 ± 35
KK 084−2−785	10 05 35.8	−07 44 06	23.31	−6.62	0.68	1.68	856 ± 24
KK 084−3−705	10 05 35.7	−07 44 25	22.28	−7.65	0.73	1.87	670 ± 31
KK 084−3−830	10 05 35.0	−07 44 59	20.82	−9.11	0.57	1.74	594 ± 32
KK 084−3−917	10 05 36.5	−07 45 16	22.94	−6.99	0.53	1.63	619 ± 28
KK 084−4−666	10 05 31.5	−07 45 03	22.47	−7.46	0.91	2.10	678 ± 21
KK 084−12n	10 05 36.8	−07 45 54	23.00	−6.93	...	1.49	911 ± 40
KK 084−36n	10 05 25.6	−07 42 33	23.02	−6.91	...	2.28	1210 ± 27
UGC 3755−2−652	07 13 50.1	+10 32 15	21.48	−7.87	1.11	1.82	323 ± 21
UGC 3755−2−675	07 13 50.4	+10 31 49	23.65	−5.70	0.81	1.53	367 ± 21
UGC 3755−2−863	07 13 51.3	+10 31 45	22.79	−6.56	1.13	1.89	290 ± 33
UGC 3755−3−914	07 13 51.4	+10 31 35	21.74	−7.61	0.75	1.31	284 ± 24
UGC 3755−3−1182	07 13 51.5	+10 31 26	20.61	−8.74	0.56	0.88	335 ± 32
UGC 3755−3−1257	07 13 52.3	+10 31 24	20.98	−8.37	1.10	1.76	327 ± 31
UGC 3755−3−2123	07 13 52.5	+10 31 01	21.36	−7.99	0.53	0.70	329 ± 22
UGC 3755−3−2363	07 13 52.2	+10 30 45	21.60	−7.75	0.76	1.00	312 ± 18
UGC 3755−3−2168	07 13 51.4	+10 30 58	21.84	−7.51	0.88	1.56	324 ± 28
UGC 3755−3−2459	07 13 52.2	+10 30 35	20.93	−8.42	0.32	0.81	333 ± 32
E490−017−3−2035	06 37 57.3	−25 59 59	21.16	−6.97	0.33	0.74	529 ± 34
E490−017−3−1861	06 37 57.3	−26 00 13	21.45	−6.68	0.50	1.57	522 ± 9

Notes.—Columns contain the following data: (1) object; (2) and (3) equatorial coordinates; (4) integrated B magnitude from our FORS2 photometry corrected for Galactic extinction (Schlegel et al. 1998); (5) absolute magnitude computed with the distances from Table 1; (6) and (7) integrated $B - V$ and $B - I$ colors corrected for Galactic extinction (Schlegel et al. 1998); (8) heliocentric radial velocities measured in this study. Units of right ascension are hours, minutes, and seconds, and units of declination are degrees, arcminutes, and arcseconds.

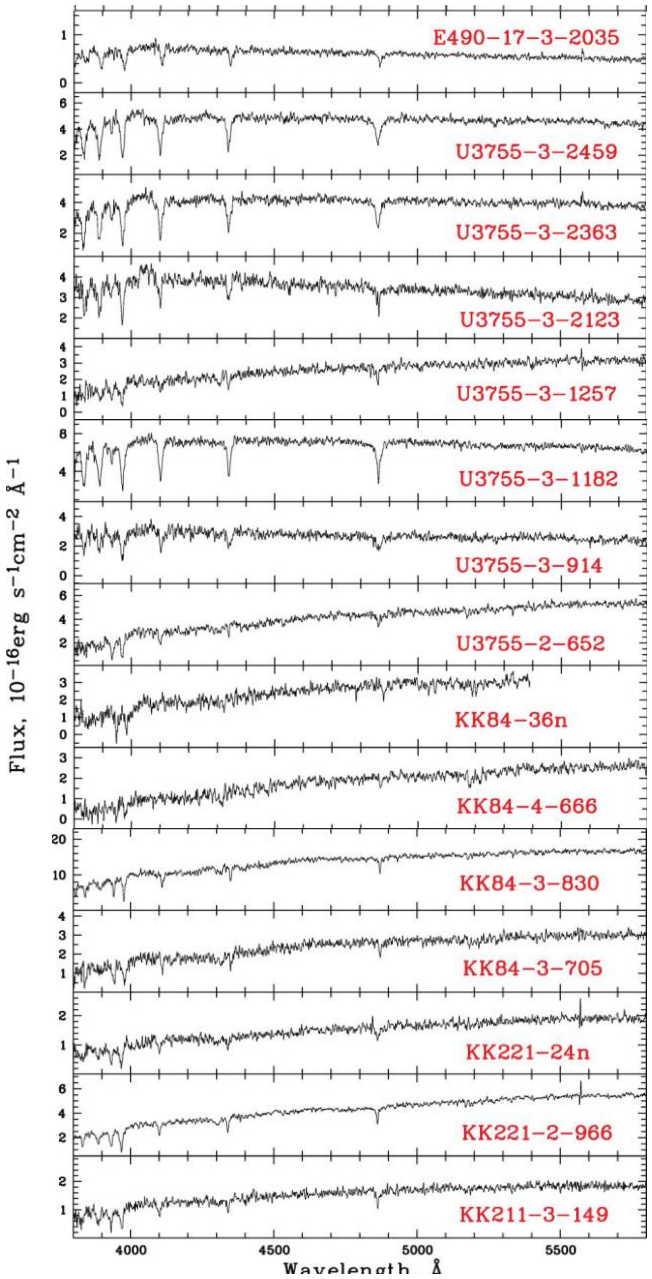

FIG. 1.— Flux-calibrated spectra of GCs in our sample dwarf galaxies.

The distribution of confirmed GCs in the color-magnitude diagram is illustrated in Figure 3 where we compare our sample with the distribution of Milky Way and M31 GCs. The bulk of our sample has $B - I$ colors very similar to the Local Group GCs. A few GC have relatively blue colors which suggests younger ages. Our sample GCs probe the luminosity range around the turnover magnitude of the GC luminosity function (GCLF). The turnover for old GC populations is expected at $M_B \approx -7.1$, assuming $M_V \simeq -7.66 \pm 0.11$ from Di Criscienzo et al. [2006] for metal-poor Milky Way GCs and a typical $B - V \approx 0.5$–0.7 for metal-poor stellar populations from Bruzual & Charlot [2003] SSP models) down to about a factor of 2–3 fainter clusters. We recall that SPM05 found indications for an excess cluster population in this magnitude range (see also van den Bergh 2007; Jordán et al. 2007), and we point out that a significant number of GC candidates from the SPM05 sample are being confirmed as genuine GCs at these faint magnitudes. However, a larger sample is required

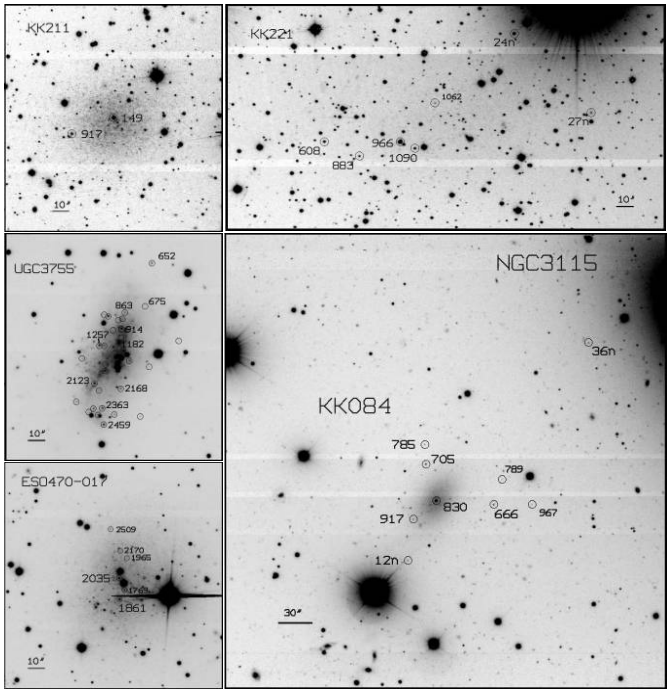

FIG. 2.— FORS-2 images of our sample dwarf galaxies with marked GCs. North is to the top, and east is on the left. The objects are labeled according to Table 5.

to robustly quantify the excess of clusters with respect to GC systems of more massive galaxies, such as the two Local Group spirals.

3. ANALYSIS

3.1. *Lick Index Measurement and Calibration*

We measure Lick indices with the routine described in Puzia et al. (2002) and P04 for GCs with spectra with S/N ≥ 30 Å^{-1}.

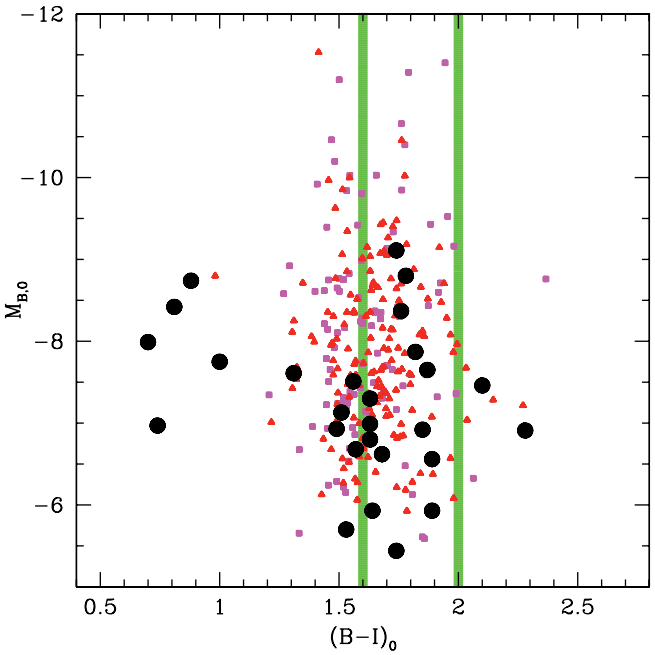

FIG. 3.— Color-magnitude diagram of confirmed GCs in LSB dwarf galaxies (*large circles*). Overplotted are also Milky Way (*small squares*) and M31 GCs (*small triangles*). The photometry for Milky Way GC was taken from the McMaster catalog (Harris 1991), while the M31 data was adopted from Barmby et al. (2000). The two vertical lines indicate the location of the blue and red GC subpopulations in giant elliptical galaxies (e.g., Puzia et al. 2004).

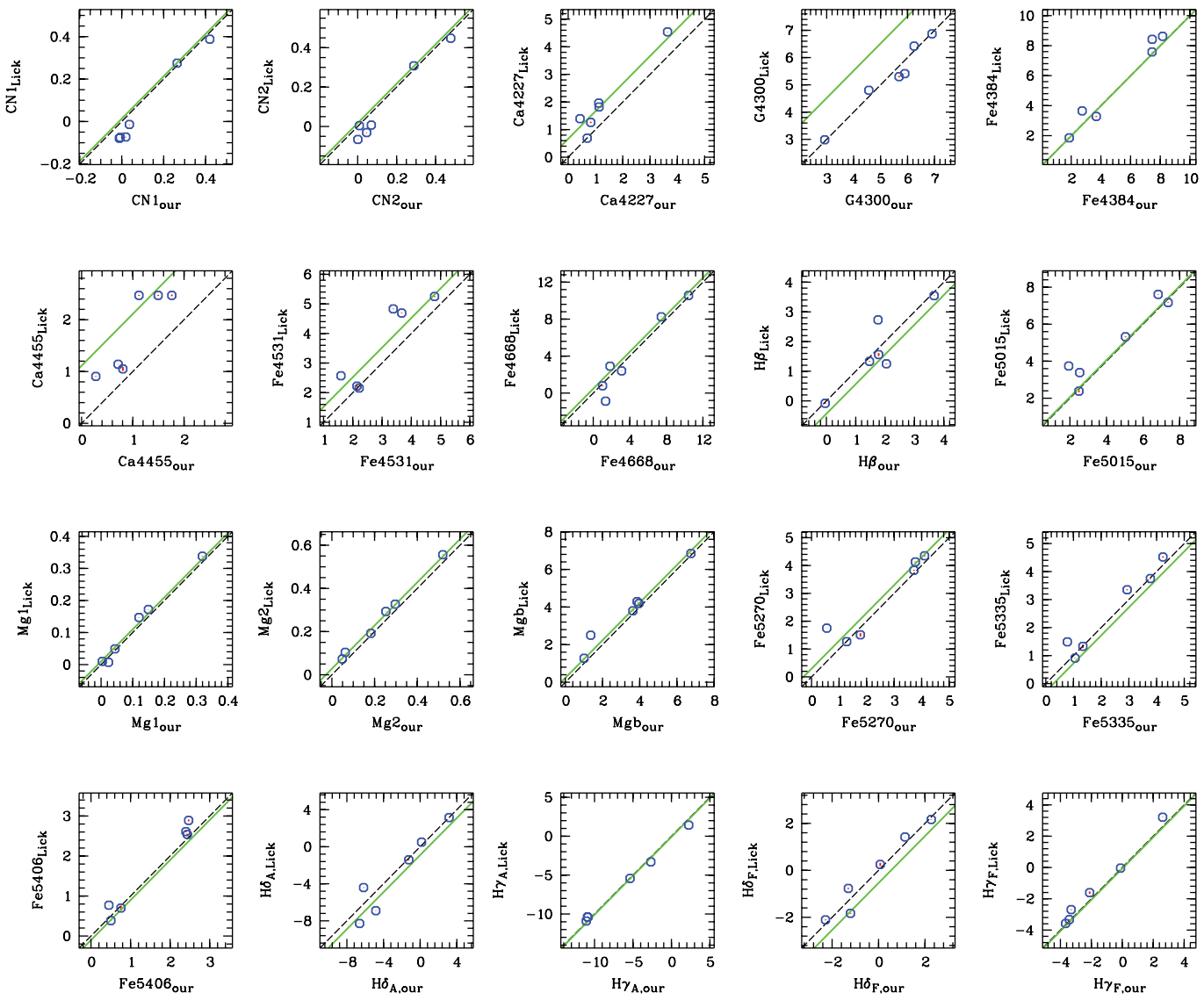

FIG. 4.—Comparison of passband measurements of our spectra and original Lick data for 10 Lick standard stars. The dashed line shows the one-to-one relation. The gray line shows the relation from P04.

In general, we select high-quality spectra for the subsequent analysis of evolutionary parameters, but include in some interesting cases a few lower S/N spectra.

P04 calibrated the instrumental FORS/MXU system of Lick line indices into the standard one using a set of 31 Lick standard stars. The correction functions were calculated in the form

$$I_{\rm cal} = I_{\rm raw} + \alpha,$$

where $I_{\rm cal}$ and $I_{\rm raw}$ are the calibrated and the measured indices, respectively. To check the correspondence of our index measurements to the Lick standard system we performed the same analysis using 10 stars observed together with our target sample. It should be noted that all standard star spectra were observed with the same slit size (1″) and were extracted and smoothed in the same way as the GCs of our study and as it was done by P04. We show comparison of passband measurements of our spectra and original Lick data for our sample Lick standard stars in Figure 4. The dashed line shows the one-to-one relation. The dotted line shows the relation from P04. Table 6 summarizes the coefficients of transformation into the Lick standard system and the rms of the calibration. Comparison of our calibration coefficients with the ones form P04 shows that in all cases but one the transformations agree well within the errors. A large difference exists for the index G4300. However, P04 noticed that this index is very noisy and its calibration uncertain. It is worth to note that the rms errors of transformations into the Lick system are large for some other indices (e.g., Ca4455; see Table 6 this paper and Table 8 in P04). However, the most important indices for our analysis, such as Hβ, Hγ_A, Hδ_A, Mg$_1$, Mg$_2$, and Mg b, Fe5270, and Fe5335 have all very robust Lick system calibrations which agree well with previous work. The calibrated Lick indices for all confirmed GCs in our sample are summarized in Table 10.

3.2. *Ages and Metallicities*

It was shown in series of papers (see, e.g., P04; Puzia et al. 2005a, 2005b) that age-metallicity diagnostic plots that make use of different Balmer indices and the composite metallicity index [MgFe]′[10]

[10] This composite Lick index is defined to be [α/Fe]-insensitive, $[{\rm MgFe}]' = \{{\rm Mg}\ b \times (0.72 \times {\rm Fe5270} + 0.28 \times {\rm Fe5335})\}^{1/2}$, see Thomas et al. (2003) for details.

TABLE 6
CORRECTION TERMS OF THE TRANSFORMATION TO THE LICK/IDS STANDARD SYSTEM (WORTHEY 1994; WORTHEY & OTTAVIANI 1997)

Index	c	rms Error	Units
CN_1	−0.067	0.028	mag
CN_2	−0.050	0.039	mag
Ca4227	0.487	0.247	Å
G4300	0.049	0.608	Å
Fe4384	0.041	0.542	Å
Ca4455	0.419	0.380	Å
Fe4531	0.322	0.762	Å
Fe4668	0.685	0.782	Å
$H\beta$	−0.183	0.277	Å
Fe5015	0.460	0.640	Å
Mg_1	0.010	0.007	mag
Mg_2	0.027	0.010	mag
Mg b	0.351	0.134	Å
Fe5270	0.345	0.203	Å
Fe5335	−0.156	0.230	Å
Fe5406	−0.208	0.124	Å
$H\delta_A$	−0.109	0.772	Å
$H\gamma_A$	−0.000	0.129	Å
$H\delta_F$	0.013	0.229	Å
$H\gamma_F$	0.491	0.148	Å

NOTE.—From Worthey (1994) and Worthey & Ottaviani (1997).

represent a powerful tool to estimate ages and metallicities of globular clusters. For data with S/N $\gtrsim 25$ Å^{-1} the Balmer index $H\gamma_A$ is most sensitive to age and least sensitive to metallicity and [α/Fe] variations, as well as the degeneracy between these parameters (Puzia et al. 2005b). The SSP model predictions of Thomas et al. (2003, 2004) for stellar populations with well-defined [α/Fe] ratios provide us with the option to estimate [α/Fe] ratio from Mg_2 versus $\langle Fe\rangle = (Fe5270 + Fe5335)/2$ diagnostic plots.

In Figure 5 we show age-metallicity diagnostic plots for our sample globular clusters with the highest S/N spectra. Almost all clusters have indices consistent with low metallicities, typically $[Z/H] \leq -1$, and a wide range of ages and [α/Fe] ratios. We compare the index measurements of our sample GCs with those of GCs in the Milky Way (Puzia et al. 2002; Schiavon et al. 2005), M31 (Puzia et al. 2005a), and the Large Magellanic Cloud (Beasley et al. 2002), and find that most objects in our sample have Balmer line indices, at a given [MgFe]′ that are comparable with metal-poor GCs in the Milky Way and M31 in all diagnostic plots of Figure 5. Several GCs in UGC 3755, which show stronger Balmer indices, resemble the subpopulation of young star clusters in the LMC (e.g., Kerber et al. 2007).

Iterating between the diagnostic plots in Figure 5 converges to give accurate metallicity and [α/Fe] estimates, as well as robust relative ages that allow one to distinguish between old, intermediate-age, and young stellar populations. We refer to this approach as the iterative technique. Another way to obtain age, metallicity, and [α/Fe] estimates is by means of linear interpolation within this three-dimensional space defined in the models and the subsequent χ^2 minimization of the difference between observed and predicted indices (Sharina et al. 2006). This technique makes use of multiple Lick indices.

We apply both techniques to our data set and summarize the results in Table 7. We show a comparison of the output results of the two techniques in Figure 6 and find good agreement for age and metallicity estimates with a scatter about the one-to-one relation that is consistent with the measurement uncertainties. The χ^2 minimization technique appears to deliver a limited range of [α/Fe] values compared to the iterative approach, which provides results more consistent with the general distribution of data in diagnostic plots of Figure 5. The χ^2 technique works entirely within the parameter space defined by the model grids. The fact that it does not make use of extrapolations in the [α/Fe] grid is likely the reason for the reduced [α/Fe] dynamic range.

3.2.1. *GCs in KK 084*

All observed globular clusters in this galaxy are old with ages >8 Gyr. The central GC in KK 84, KK 084−3−830, has the lowest metallicity and the oldest age among all GCs in this galaxy. We find two metal-poor $[Z/H] \approx -1.4$) and two metal-rich clusters $[Z/H] \approx -0.3$). Both metal-rich clusters (KK 84−36n and KK 84−666) are located near NGC 3115 (see Fig. 1) and have elevated radial velocities, which grants the possibility that they might be associated with the disk component of NGC 3115 rather than KK 084. Our results for these two GCs are also in line with the VLT study of GCs in NGC 3115 by Kuntschner et al. (2002) and GMOS spectroscopy data for the diffuse light of NGC 3115 by Norris et al. (2006). Kuntschner et al. found two GC subpopulations with mean metallicities $[Fe/H] \simeq -0.37$ and −1.36 dex. The absolute age was found 11–12 Gyr for all observed GCs. The long-slit spectroscopy of the diffuse light in NGC 3115 by Norris et al. shows a luminosity-weighted age of ∼6 Gyr for the disk component and a luminosity-weighted age of ∼12 Gyr for the spheroid.

3.2.2. *GCs in UGC 3755*

GCs 1182, 2363, 2459, and 914 in the isolated dwarf irregular galaxy UGC 3755 appear to be the youngest objects in our sample with ages in the range 1–4 Gyr. The other clusters in UGC 3755 are significantly older. One noteworthy case is U3755−3−1257, which shows an intermediate age and metallicity. The youngest GC in our sample has the smallest projected distance relative to the photometric center of the host galaxy.

3.2.3. *GCs in ESO 490−17*

The two GCs in our sample that are associated with ESO 490-17 are both metal-poor. Although our data for this galaxy has the lowest S/N, the age difference between the two GCs with high-quality spectra is seen clearly in the diagnostic plots of Figure 5. This difference is reflected in the integrated colors (see Table 5). In terms of projected distance, the young cluster GC 2035 is located closer to the galaxy center.

3.2.4. *GCs in KK 211*

We find another intermediate-age GCs (6 ± 2 Gyr) in KK 211, which appears to be the central star cluster of this dSph galaxy. The cluster age and metallicity estimates are consistent with the brightest intermediate-age AGB stars in this galaxy, 4 ± 1 Gyr, $[Fe/H] = -1.4 \pm 0.2$, measured by Rejkuba et al. (2005).

3.2.5. *GCs in KK 221*

The two brightest GCs in KK 221 are old ($t > 10$ Gyr) and metal-poor $[Z/H] \lesssim -1.5$). It is difficult to assess whether these objects are associated with the center of K221 due to the very faint surface brightness profile of the host galaxy. However, both seem to be gravitationally bound judging from their radial velocities.

A mean radial velocity of all GCs in KK 221 coincides well with the radial velocity of the brightest GC. We find a radial velocity anisotropy (rotation) among the GCs at the 95% confidence level, in the sense that the radial velocities of GCs 608, 883, and 966 located in the western edge of KK 221 differ systematically

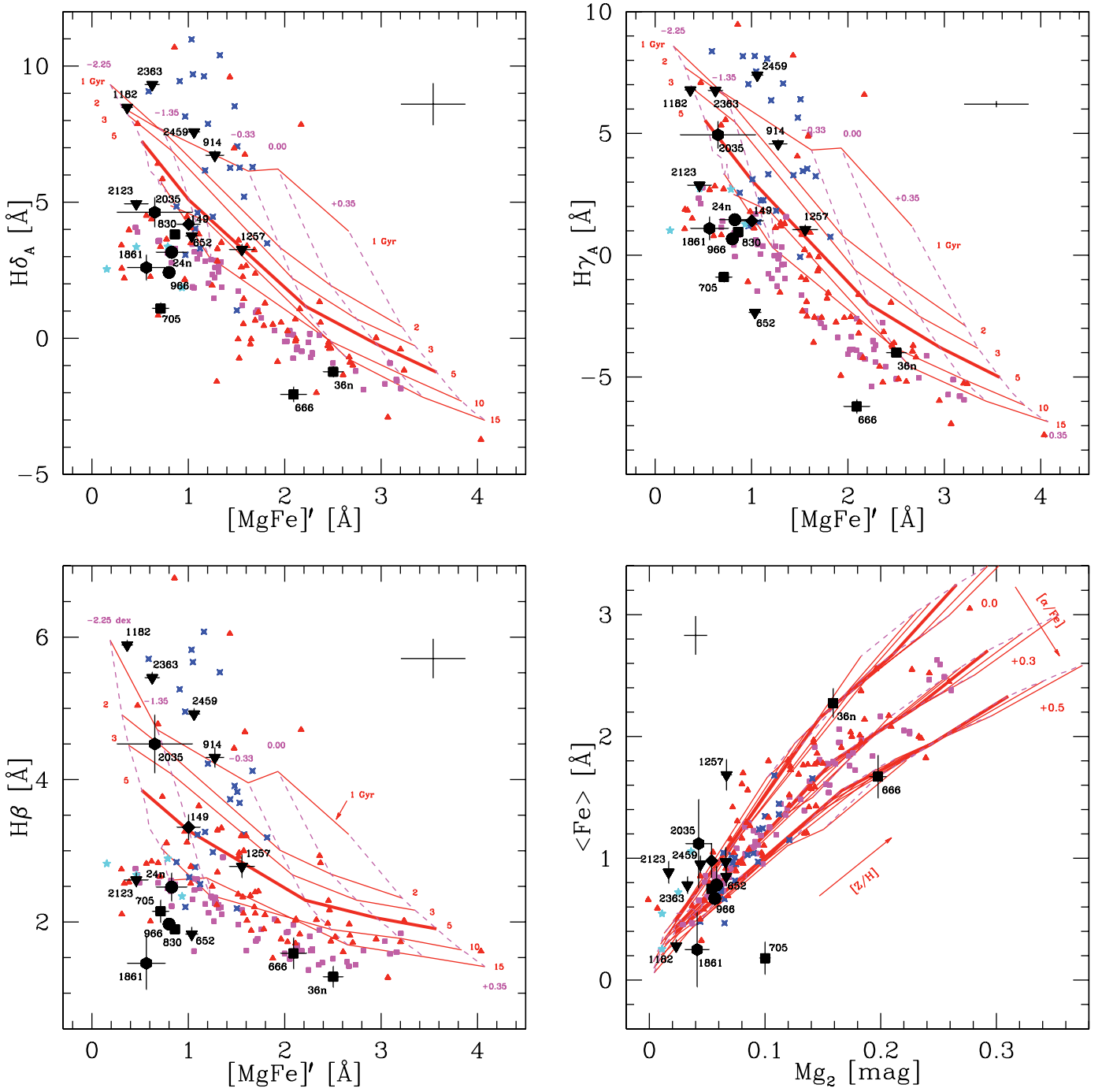

FIG. 5.—Diagnostic plots for globular clusters in KK 084 (*squares*), GC 149 KK 211 (*diamond*), GCs 966 and 24n in KK 221 (*circles*), GCs 2035 and 1861 in E490−17 (*hexagons*), and GCs in UGC 3755 (*inverted triangles*). We use SSP model predictions from Thomas et al. (2003, 2004). The Balmer line index diagnostic plots (*both top panels and the bottom left panel*) show the grids for $[\alpha/\mathrm{Fe}] = 0.3$ dex. The cross in the corner of each panel indicates the systematic calibration uncertainty to the Lick index system. The error bars of individual GCs are the total statistical uncertainties. Overplotted are Lick index measurements for GCs in the Milky Way (*small squares*; Puzia et al. 2002; Schiavon et al. 2005), M31 (*small triangles*; Puzia et al. 2005a), the Large Magellanic Cloud (*small four-pointed stars*; Beasley et al. 2002), and the Fornax dSph galaxy in the Local Group (*small five-pointed stars*; Strader et al. 2003a).

from the radial velocities of GCs 1090, 24n, and 27n located in the eastern edge of the galaxy.

3.3. [α/Fe] *Ratios*

Because of different progenitor lifetimes Type II and Type Ia supernovae enrich their ambient medium on different timescales. In consequence the chemical composition of stellar populations, together with their ages and metallicities, can be used to constrain their formation timescales. One good way to do so is to measure the [α/Fe] ratios of stellar populations. Massive stars that live up to a few 100 Myr enrich the interstellar medium predominantly with α-elements (Woosley et al. 2002), while Type Ia supernovae are delayed by 1–3 Gyr and eject mainly iron-peak elements (Nomoto et al. 1997).

Besides ages and metallicities our fitting routines simultaneously determine [α/Fe] ratios for all sample clusters. However, the resolution of the [α/Fe] diagnostic grid decreases toward lower metallicities. Most of our sample GCs have relatively low [Z/H]

TABLE 7
AGES, [Z/H] AND [α/Fe] FOR OUR SAMPLE GLOBULAR CLUSTERS

Object	Age_{χ^2} (Gyr)	[Z/H] (dex)	[α/Fe] (dex)	Age_I (Gyr)	$[Z/H]_I$ (dex)	$[\alpha/Fe]_I$ (dex)
KK 211−3−149	6 ± 2	−1.4 ± 0.3	0.1 ± 0.3	$7.4^{3.1}_{1.4}$	$-1.45^{0.15}_{0.13}$	$-0.27^{0.20}_{0.23}$
KK 221−2−966	10 ± 2	−1.6 ± 0.1	0.1 ± 0.3	$11.7^{0.2}_{0.1}$	$-1.47^{0.04}_{0.02}$	$0.51^{0.08}_{0.08}$
KK 221−24n	9 ± 2	−1.7 ± 0.3	0.3 ± 0.4	$11.4^{1.1}_{1.0}$	$-1.58^{0.16}_{0.02}$	$0.28^{0.21}_{0.22}$
KK 084−3−705	9 ± 1	−1.2 ± 0.1	0.3 ± 0.2	$12.1^{0.2}_{0.2}$	$-1.16^{0.07}_{0.06}$	$0.99^{0.02}_{0.02}$
KK 084−3−830	10 ± 4	−1.6 ± 0.1	0.3 ± 0.2	$10.2^{0.9}_{0.1}$	$-1.45^{0.02}_{0.24}$	$0.25^{0.07}_{0.07}$
KK 084−4−666	8 ± 3	−0.1 ± 0.2	0.3 ± 0.2	$14.4^{0.6}_{0.6}$	$-0.31^{0.03}_{0.03}$	$0.52^{0.07}_{0.06}$
KK 084−36n	8 ± 2	−0.5 ± 0.2	0.1 ± 0.2	$10.7^{1.7}_{1.2}$	$-0.30^{0.05}_{0.05}$	$-0.05^{0.05}_{0.04}$
U3755−2−652	8 ± 2	−1.3 ± 0.2	0.1 ± 0.1	$10.6^{0.9}_{0.4}$	$-0.94^{0.03}_{0.02}$	$0.32^{0.09}_{0.09}$
U3755−3−914	4 ± 1	−1.3 ± 0.1	0.0:	$1.1^{0.2}_{0.2}$	$-0.48^{0.03}_{0.07}$	$0.17^{0.07}_{0.08}$
U3755−3v1182	2 ± 1	−1.8 ± 0.4	0.1 ± 0.4	$2.3^{0.2}_{1.2}$	$-2.07^{0.58}_{0.09}$	$0.69^{0.09}_{0.10}$
U3755−3−1257	7 ± 2	−1.2 ± 0.2	0.1 ± 0.1	$3.2^{0.9}_{0.6}$	$-0.55^{0.07}_{0.10}$	$-0.55^{0.08}_{0.08}$
U3755−3−2123	6 ± 2	−1.8 ± 0.3	0.1 ± 0.4	$14.0^{0.3}_{2.6}$	$-2.24^{0.18}_{0.02}$	$-0.41^{0.06}_{0.02}$
U3755−3−2363	2 ± 2	−1.3 ± 0.2	0.1 ± 0.1	$0.9^{0.2}_{0.6}$	$-0.90^{0.31}_{0.07}$	$-0.11^{0.06}_{0.06}$
U3755−3−2459	1 ± 1	−1.3 ± 0.1	0.4 ± 0.2	$0.6^{0.1}_{0.1}$	$-0.36^{0.02}_{0.02}$	$-0.04^{0.03}_{0.03}$
E490−17−2035	4 ± 2	−1.4 ± 0.2	0.1 ± 0.1	$7.2^{1.0}_{3.7}$	$-1.73^{0.89}_{0.29}$	$-0.34^{0.37}_{0.14}$
E490−17−1861	9 ± 4	−1.7 ± 0.3	0.5:	$11.7^{0.7}_{1.0}$	$-1.53^{0.11}_{0.04}$	$0.99^{0.02}_{0.45}$
Mean ± error	6.4 ± 0.7	−1.33 ± 0.11	0.19 ± 0.04	8.1 ± 1.2	−1.16 ± 0.16	0.18 ± 0.12
Standard deviation σ	3.0	0.46	0.14	4.9	0.63	0.47
Median ± 25 percentile	8.0 ± 2.5	−1.3 ± 0.2	0.1 ± 0.1	10.6 ± 4.3	−1.16 ± 0.53	0.25 ± 0.32

NOTES.—Determined using our χ^2 minimization code and the iterative interpolation routine. The bottom of the table shows the statistics of our sample, i.e., the mean and its error, standard deviation, weighted mean and the corresponding standard deviation, as well as the median and its 25 percentile margin. See text for details.

values and the accuracy of [α/Fe] values is reflected by the range of uncertainties, typically ∼0.1−0.3 dex (see Fig. 5 and Table 7). Our sample covers a wide range in [α/Fe] much broader than what is expected from the average measurement uncertainty and, thus, implies significant chemical variance in the GC systems of dwarf galaxies. The mean [α/Fe] for our sample is consistent with enhanced values with $\langle[\alpha/Fe]\rangle = 0.19 \pm 0.04$ for the χ^2 technique and 0.18 ± 0.12 for the iterative approach. This compares well with values of GCs in the Fornax dSph galaxy in the outskirts of the Milky Way (Strader et al. 2003a).

Interestingly, the mean [α/Fe] of GCs in UGC 3755 is systematically lower than that of the rest of the sample. For the mean [α/Fe] of UGC 3755, we find $\langle[\alpha/Fe]\rangle = 0.13 \pm 0.05$ using the χ^2 technique and 0.01 ± 0.16 with the iterative approach, while the rest of the sample has $\langle[\alpha/Fe]\rangle = 0.23 \pm 0.05$ using the χ^2 technique and 0.32 ± 0.16 using the iterative approach. In each case, this is a $\sim 2\,\sigma$ offset. In particular, the youngest GCs in UGC 3755 have the lowest [α/Fe] ratios, but the small number statistics of this subsample makes the age-[α/Fe] correlation marginally significant and we do not attempt to quantify this trend.

The two most metal-rich GCs, KK 84−666 and KK 84−36n, are an interesting pair in terms of their [α/Fe] ratios. Although KK 84−666 has roughly solar metallicity (see Table 7) its α-element enhancement is relatively high, and comparable to those of Local Group GCs. KK 84−36n, on the other hand, which has the second highest metallicity in our sample shows almost no α-element enhancement, and clearly stands out compared with the rest of GCs in KK 84. Together with its location, which puts it closer to NGC 3115 than KK 84 (in terms of projected distance), its low [α/Fe] ratio is yet another piece of evidence that this GCs is likely a member of the extended disk of NGC 3115 (see also § 3.2.1).

We observe a relatively large fraction of low-[α/Fe] GCs which are less frequent in the GC systems of Local Group spirals. In our sample 44% ± 17% of GCs have subsolar [α/Fe] ratios. In comparison, only ∼20%−30% of GCs in the two Local Group spirals Milky Way and M31 which had their [α/Fe] determined with the same technique have subsolar [α/Fe] values (Puzia et al. 2006). We point out that the sampled age, metallicity, and luminosity ranges for GCs in nearby low surface brightness (LSB) dwarf galaxies and Local Group spirals are not the same and that correlations between the [α/Fe] and any of these parameters will likely alter the observed fraction of subsolar [α/Fe] clusters. If we restrict the Local Group spiral GC sample to intermediate and faint luminosity ($M_B \gtrsim -8$), old ($t > 8$ Gyr), and metal-poor GCs ($[Z/H] < -1$)—the typical regime of our observed sample-the fraction of subsolar [α/Fe] clusters drops to ∼15%, which is about 1.7 σ off compared to the fraction in our sample. The work of Pritzl et al. (2005), which derives mean [α/Fe] ratios for Milky Way GCs from high-resolution spectroscopy of individual member stars shows an even lower fraction of ∼2%. Although this is the most representative comparison we can perform at the current state (given the limited sample statistics), we stress that GCs in dwarf and spiral galaxies are likely to have experienced different dynamical evolution histories. Star clusters of similar luminosity (mass) we observe today may have started off with very different initial masses. However, since only the most massive GCs are prone to self-enrichment (such as ω Cen; e.g., Recchi & Danziger 2005; Villanova et al. 2007), the GCs in our sample should reflect the global chemical composition at the time of their formation, independent of their mass. Hence, we speculate that the somewhat lower fraction of Milky Way GCs with subsolar [α/Fe] may be an indication for significantly shorter star formation and enrichment timescales compared to those in field dwarf galaxies.

3.4. *Other Abundances*

We conducted a detailed investigation of numerous other Lick index diagnostic diagrams. In Figure 7 we show diagnostic plots for indices that are sensitive to the abundance of carbon, nitrogen, and calcium (Tripicco & Bell 1995). Because a strict quantitative analysis is not possible due to a lack of corresponding model predictions, we focus the following discussion on qualitative trends.

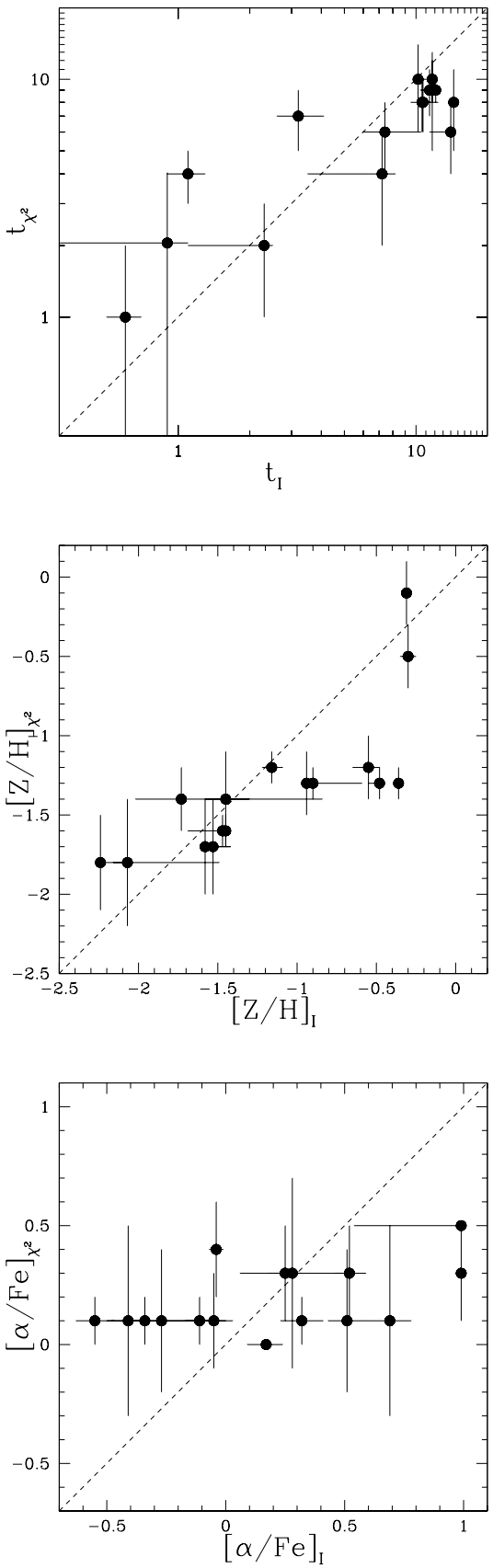

FIG. 6.—Comparison of ages, [Z/H] and [α/Fe] values for our sample GCs that were derived using the iterative and χ^2 minimization technique. All measurements are summarized in Table 7.

3.4.1. *Carbon and Nitrogen*

The CN_2 versus [MgFe]′ diagram (*top left panel*) shows significant scatter in CN index strength for our sample GCs, mostly "below" the model grid toward lower CN_2 index values. At metallicities typical for our sample GCs, this scatter cannot be accounted for by [α/Fe] variations alone as it is demonstrated in the Figure 7 by the two grid of population synthesis models for [α/Fe] ratios of 0.0 and +0.5 dex. It requires additional variance in, at least, one other element abundance to which the CN_2 index is sensitive to match the observed distribution. To qualitatively test this hypothesis we explore the influence of carbon and nitrogen enhancement on the model grid using the predictions for C and N-enhanced models from Thomas et al. (2003). We overplot two isochrones for a factor of 3 enhanced C and N abundance at $[\alpha/\mathrm{Fe}] = 0.5$ for a 5 Gyr old stellar population. We recall that the corresponding predictions for nonenhanced populations are plotted as thick lines in the two grids. The shape of the C/N-enhanced model grid is very similar to that of the nonenhanced predictions and for clarity reasons we avoid plotting the entire grid for the C/N-enhanced populations, and note that age and metallicity are highly degenerate in these grids and that both parameters have no impact on the following discussion.

The comparison of the enhanced models with our data in the CN_2 versus [MgFe]′ diagram shows that some GCs in dwarf galaxies appear to be highly underabundant in C and/or N. This is particularly the case for GCs in UGC 3755, which exhibit on average significantly lower CN_2 index values. However, from the variations in CN_2 index strength alone we cannot decide whether chemical variance in carbon and/or nitrogen is responsible for the offsets.

A sanity check is provided by the $C_2$4668 and G4300 versus [MgFe]′ diagrams which are both mildly sensitive to C abundance but not sensitive to N variations (Tripicco & Bell 1995). Most GCs in the $C_2$4668 and G4300 versus [MgFe]′ diagrams show relatively little deviations from the general trend of model predictions, and we infer that the abundance of carbon is less likely to change with respect to predictions of standard population synthesis models than the nitrogen abundance, which implies that the nitrogen abundance appears to vary significantly in GC systems of dwarf galaxies. We suggest that this pure qualitative result is being confirmed with higher resolution spectroscopic observations.

3.4.2. *Calcium*

In the Ca4227 versus [MgFe]′ diagram we add a model which describes a stellar population with a factor of 3 calcium underabundance relative to the other α-elements. In the Ca4227 versus [MgFe]′ plot (Fig. 7, *bottom right panel*) many GCs in our sample show excess in Ca4227 index strength. The overplotted model for $[\alpha/\mathrm{Ca}] = 0.5$ indicates that this offset may be due to a Ca enhancement in some GCs. As the absolute calibration of Ca abundance model predictions is still uncertain (see Cenarro et al. 2004; Prochaska et al. 2005), we merely point out this rather intriguing abundance pattern should be checked with higher resolution spectra.

4. DISCUSSION

4.1. *Chemical Tagging of GCs in LSB Dwarf Galaxies*

The variance of GC chemical compositions in and outside the Local Group reveals complex enrichment histories. The *old* GCs in our sample with ages $t \gtrsim 8$ Gyr show marginally different [α/Fe] ratios[11] compared to the typical old GCs in the Local Group,

[11] $\langle[\alpha/\mathrm{Fe}]\rangle = 0.21 \pm 0.04$ using the χ^2 technique and 0.25 ± 0.15 dex for the iterative approach.

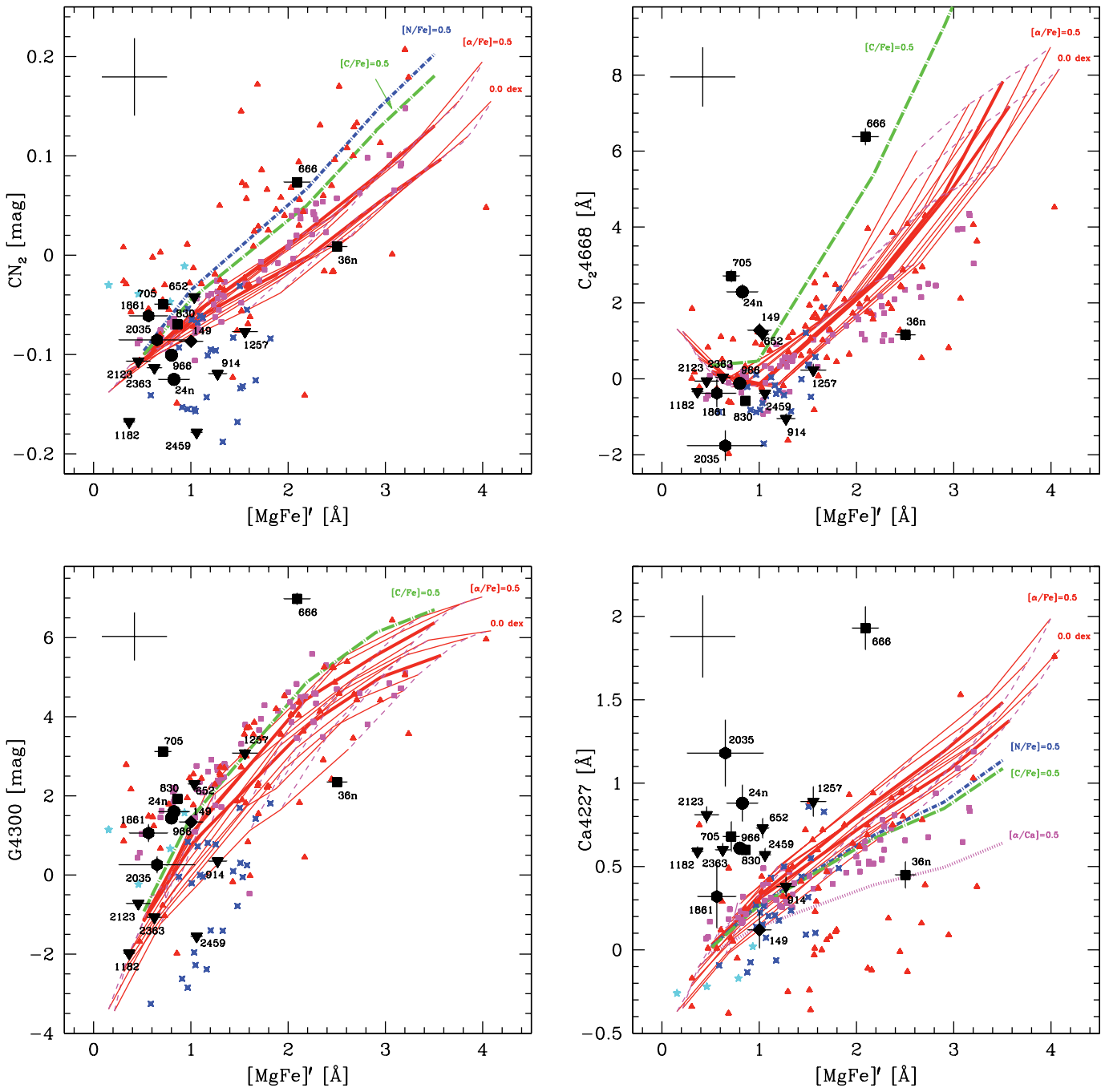

FIG. 7.—Diagnostic plot of [MgFe]′ vs. indices primarily sensitive to C, N, and Ca abundances. We plot two model grid for $[\alpha/\mathrm{Fe}] = 0.0$ and 0.5 dex, and all ages and metallicities as in Fig. 5. Note the offset in CN between younger UGC 3755 GCs and other GCs.

which are α-enhanced at 0.29 ± 0.01 dex (leaving out Pal12, Ter7, Rup106, and M68, see Pritzl et al. 2005 for details). The younger GCs in our sample with ages $t \lesssim 8$ Gyr have significantly lower $[\alpha/\mathrm{Fe}]$ ratios[12] and are comparable to Milky Way GCs associated with the Sagittarius remnant and other distinct GCs such as Ruprecht 106, ω Centauri, and NCG 2419, which have $\langle[\alpha/\mathrm{Fe}]\rangle = 0.06 \pm 0.05$ (Pritzl et al. 2005).

Solar-type $[\alpha/\mathrm{Fe}]$ ratios are consistent with star formation timescales longer than $\sim$1–3 Gyr, when ejecta of Type II *and* Type Ia supernovae are fully mixed in the interstellar medium (Greggio 2005). $[\alpha/\mathrm{Fe}]$ ratios at $\sim$0.3 dex indicate shorter and more intense cluster formation, on timescales of the order of a few hundred million years. This, in turn, suggest that some of the oldest GCs in our sample were formed relatively early, at similar epochs as the typical Milky Way GC. Less α-enhanced GCs, on the other hand, likely formed $\gtrsim$1 Gyr after the big bang at $z \approx 5.7$ or later, which would place their formation period at the end of reionization or thereafter (e.g., Kashikawa et al. 2006; Benson et al. 2006).

The characteristic chemical compositions limit the fraction of accreted GCs from satellite LSB-type galaxies during the assembly process of Local Group spirals galaxies. Given the difference in α-enhanced to non-α-enhanced GCs between our sample and

[12] $\langle[\alpha/\mathrm{Fe}]\rangle = 0.14 \pm 0.07$ using the χ^2 technique and 0.03 ± 0.20 dex for the iterative approach.

the Local Group spirals (see § 3.3), our results imply that to qualify as potential building block for the two massive Local Group spirals in the hierarchical picture of galaxy formation, LSB dwarf galaxies would either have to (1) cease forming star clusters long before the beginning of enrichment by Type Ia supernovae before being accreted much later by a more massive halo or (2) being accreted when the gas out of which star clusters were forming was still not polluted by Type Ia supernovae.

Other element abundance ratios provide us with the opportunity to chemically tag GCs that were formed in the field environment and later accreted by more massive galaxy halos, much like the chemical tagging of accreted stellar subpopulations that are part of the diffuse-light component in nearby galaxies (Freeman & Bland-Hawthorn 2002; Geisler et al. 2007). For instance, at a given [MgFe]′ index (i.e., total metallicity) the carbon and nitrogen enhancement of our sample GCs is consistent with that of Galactic GCs, but fails to match the chemical composition of M31 GCs which have excess CN_2 indices (see Fig. 7). It was shown in a series of studies that the higher CN_2 index values for old M31 GCs are due to a nitrogen enhancement by at least a factor of 3 compared to the younger cluster population (Li & Burstein 2003; Burstein et al. 2004; Beasley et al. 2005; Puzia et al. 2005a). We remind the reader that the comparison sample of M31 GCs is biased toward disk clusters and samples only poorly the halo GC population (see Fig. 1 in Puzia et al. 2005a), where accreted objects are more likely to reside. Interestingly, although the CN_2 indices of the N-enriched M31 GCs do not match our sample GCs, similar N-enhancement can be suspected in GCs of the Fornax dSph galaxy (see Fig. 7). We conclude that it is relatively unlikely that M31 accreted a significant amount GCs from satellite dwarfs similar to those in our sample on orbits close to the plane of the M31 disk. On the other hand, judging from Figure 7 the average C/Fe and N/Fe chemistry of our sample GCs appears to be similar to the one of metal-poor Milky Way GCs. We currently lack the spectroscopic database of outer-halo GCs in the two Local Group spirals to further constrain the selective accretion history of these massive spiral galaxies.

4.2. *Specific Frequencies of GCs in LSB Dwarf Galaxies*

The specific frequency, S_N (Harris & van den Bergh 1981), is defined as the number of globular clusters per unit $M_V = -15$ mag of host galaxy light: $S_N = N_{GC} \times 10^{0.4(M_V+15)}$. It is tightly related to cluster formation efficiency, which is varying as a function of host galaxy's morphological type, mass, and local environmental density (e.g., Harris 1991; Richtler 1995). Kumai et al. (1993) and West (1993) found a significant trend of increasing S_N with increasing environmental density. Another observational fact is that S_N values grow for nucleated dwarf galaxies with decreasing galactic mass (e.g., Miller et al. 1998).

Figure 8 illustrates the $M_V - S_N$ diagram, where the galaxy luminosity is plotted against the GC specific frequency. Our five sample LSB galaxies are shown as solid circles, while data for dwarf galaxies in the Virgo Cluster (Durrell et al. 1996) and more massive early-type galaxies (Harris 1991) are shown as open symbols. The solid line is a model for which $S_N \sim 0.0025 L_{gal}^{0.3}$ (McLaughlin 1999), where a constant number of GCs per unit mass is formed with an efficiency $e = 0.0025$, and the mass of gas is much lower than the stellar mass. This thin line shows the mass-loss model $S_N \sim M^{-5/3}$, which follows from $M/L_V \sim M^{2/3}$ (Dekel & Woo 2003) or $M/L \sim L^{-0.37}$ (Dekel & Silk 1986). The vertical normalization of this model is arbitrary and was chosen to fit the dwarf galaxy data.

We point out the similarity of S_N values for field and cluster dwarf galaxies at a given galaxy luminosity, especially for faint

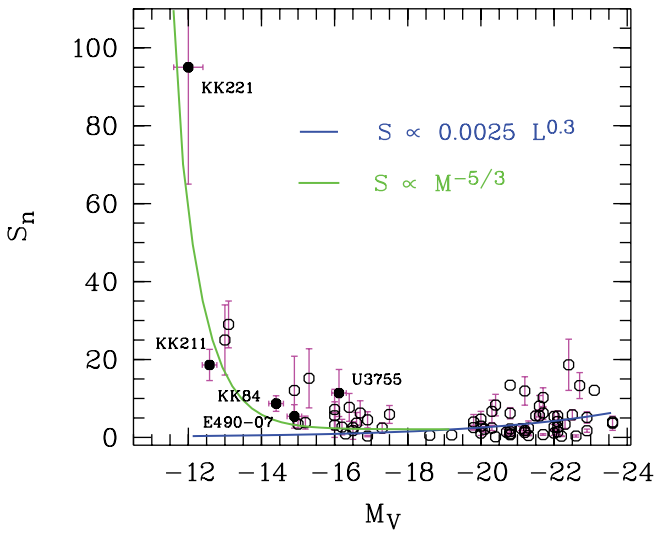

FIG. 8.—Specific frequency, S_N, vs. luminosity for galaxies from the samples of Durrell et al. (1996) and Harris (1991) (*open symbols*), and for our sample of five galaxies (*solid circles*). The dark solid line shows S_N predictions which assume that GCs were formed in galaxies in direct proportion to the initial gas mass. The light solid line shows the Dekel & Silk model of mass loss.

galaxies. Provided not a size-of-sample effect, this result implies that environment is not the driving parameter for the M_V-S_N correlation for dwarf galaxies. Less massive galaxies lose gas more efficiently because objects with shallower potential wells develop galactic winds more easily (e.g., Arimoto & Yoshii 1987; Matteucci 1994), and it seems plausible that internal factors, such as galactic winds, are shaping the $M_V - S_N$ relation of dwarf galaxies. These results require further testing with larger galaxy samples.

A particularly interesting fact is that dIrr and dSph galaxies seem to follow the same M_V-S_N trend. At face value, this appears to be in contrast with chemical evolution models and observations of abundance ratios in low-mass galaxies. For instance, Lanfranchi & Matteucci (2003) concluded that one or two long starbursts with very efficient winds well describe the chemical evolution of dSphs. On the other hand, blue compact galaxies are characterized by a star formation history proceeding in several short bursts separated by long quiescent periods. Given varying star formation histories, similar M_V-S_N relations for both dIrr and dSph galaxies require that the fading of the galaxy light and the dynamical evolution of the globular cluster system are tightly related.

Passive evolution of dIrr galaxies leads to a fading of up to ~2 mag of their integrated magnitudes if they were to abruptly stop forming stars (Hunter & Gallagher 1985). Assuming a nonchanging S_N, this requires the disruption of ~80%–90% of all formed star clusters, and is in line with observations of the so-called cluster infant mortality in nearby young star cluster systems (Chandar et al. 2006; Whitmore et al. 2007). This also suggests that the effects of tidal forces acting in group and cluster environments are linked in disrupting star clusters and their host dIrr LSB galaxies (Gnedin 2003; Georgiev et al. 2006). We suggest a detailed study of globular cluster systems in low-mass galaxies sampling galaxy mass, morphology, and environmental density to test our findings.

4.3. *Nuclei of Dwarf Galaxies*

Our spectroscopic study shows that some of the lowest mass galaxies ($M_V \approx -12$ mag) can have nuclear star clusters, i.e., the brightest GC is located near the optical center of a galaxy. The

two most prominent cases in our data set are KK 211−149, and KK 84−830. Both have low metallicities $[Z/H] \approx -1.5$, see Table 7). KK 211−149 is an intermediate-age GC, while KK 84−830 is old. Both nuclear clusters are found in dwarf galaxies located in close vicinity to massive galaxies, NGC 5128 and NGC 3115, respectively.

McLaughlin et al. (2006) have shown that the limiting mass of a central massive object in dwarf galaxies is defined as follows:

$$M_{\rm CMO} = 3.67 \times 10^8\ M_\odot\ \lambda^{-1}\ \sigma_{200}^4\ (f_g/0.16)\ , \qquad (1)$$

where λ is the massive-star feedback equal to $\sim$0.03−0.1 for a nuclear star cluster, $\sigma_{200} \equiv \sigma/200$ km s^{-1}, and the baryon fraction $f_g = \Omega_b/\Omega_m = 0.16$ (Spergel et al. 2003). So, a limiting mass of a nucleus in dSph galaxies with $\sigma \approx 10$ km s^{-1} is in the range $\sim 10^4$−$10^5\ M_\odot$, the mass range of Local Group globular clusters. We compute the total masses for both our nuclear clusters from the photometric information in Tables 5 and 7 using the population synthesis prediction of Bruzual & Charlot (2003) assuming a Salpeter initial mass function (IMF). We find $2.5 \times 10^5\ M_\odot$ for KK 211−149 and $2 \times 10^6\ M_\odot$ for KK 84−830. A more "top-heavy" IMF compared to the Salpeter IMF would bring both mass estimates in better agreement. Indications for a "top-heavy" IMF are found in the central stellar populations of the Milky Way (Nayakshin et al. 2006; Nayakshin et al. 2007). Heated molecular clouds are suspected to produce "top-heavy" IMFs due to a simultaneous increase in the thermal Jeans mass and the collisional destruction of low-mass stellar cores (Elmegreen & Shadmehri 2003).

The two nuclear star clusters are massive and compact enough to survive a Hubble time in isolated galaxies in the absence of dynamical factors, such as tidal interactions, galaxy-galaxy encounters, interaction with ISM, etc. Using the structural parameters determined in Sharina et al. (2005) and the evolution models of Fall & Zhang (2001) we compute a mass-loss of 7% for KK 211−149 and 3% for KK 84−830 over the next 12 Gyr due to two-body relaxation. Including tidal interactions on orbits typical for Milky Way GCs, as adopted by Fall & Zhang, these fractions increase by a factor of $\lesssim$2. So far we know of only one nucleated early-type dwarf galaxy (Sagittarius dSph) in the Milky Way subgroup, a few in the M31 subgroup, and none in the Canes Venatici Cloud, and among isolated nearby LV galaxies (e.g., Grebel 2006 and references therein). The absolute number of nucleated early-type dwarf galaxies is higher in denser environments, such as the Fornax and Virgo galaxy clusters (e.g., Binggeli et al. 1985; Miller et al. 1998; Côté et al. 2006; Lisker et al. 2007). Although this suggests that the process of nucleation in cluster dwarf galaxies is likely driven by dynamical factors that depend on the local environmental density, the nucleation fraction among dwarf galaxies in different environments appears to be roughly constant. Compared to the few nucleated dwarfs in the Local Group with a total mass of $M_{\rm total} \approx 2 \times 10^{12}\ M_\odot$ (Karachentsev & Kashibadze 2005; van den Bergh 2006), the Virgo galaxy cluster holds $\sim$300 nucleated dwarfs (Sandage et al. 1985) and has a total dynamical mass of $M_{\rm total} \approx 1.2 \times 10^{15}\ M_\odot$ (Fouqué et al. 2001). Hence, our back of the envelope calculation suggests similar nucleation fractions as a function of the total group/cluster mass. But, of course, these numbers are very rough, especially for the Virgo Cluster, where the number of galaxies with nuclear star clusters grows with higher spatial resolution (Côté et al. 2006). Clearly, a larger sample is necessary to assess the frequency of nuclear clusters among field dwarf galaxies.

5. CONCLUSIONS

Numerous photometric and spectroscopic studies of globular clusters in Virgo and Fornax cluster dwarf galaxies have been undertaken in the last years, which targeted bright dwarf galaxies down to $M_V \approx -15$ mag (see Miller 2006). Due to observational selection effects dwarf galaxies fainter than this are missed at distances of $D \approx 17$ Mpc. Faint LSB dwarf galaxies down to $M_V \approx -12$ mag have long been thought to be free of globular clusters, because they have insufficient mass. Our *HST* WFPC2 survey of low-mass dwarf galaxies (SPM05), situated at distances 2−6 Mpc in the Local Volume, revealed a rich population of globular cluster candidates (GCCs). In this work, we observed five of these galaxies with the VLT/FORS2 spectrograph in MXU mode and found that all targeted GCCs except one are genuine globular clusters. We could also confirm five additional globular clusters in our sample galaxies. Two clusters appear to be the nuclei of KK 84 and KK 211. The confirmed globular clusters are in general old and metal-poor, and show a range of $[\alpha/{\rm Fe}]$ ratios. The mean $\langle[\alpha/{\rm Fe}]\rangle = 0.19 \pm 0.04$ that was determined with the χ^2 minimization technique and 0.18 ± 0.12 dex which was computed using the iterative approach appears slightly lower than the mean $\langle[\alpha/{\rm Fe}]\rangle = 0.29 \pm 0.01$ for typical Milky Way clusters. Globular clusters in the two isolated, relatively bright dwarf galaxies UGC 3755 and ESO 490−17 show a wide range of ages from 1 to 9 Gyr, and imply extended star formation histories in these galaxies. This goes in hand with the measured low $[\alpha/{\rm Fe}]$ ratios for the younger clusters and is consistent with low intensity star bursts. The oldest clusters with the highest $[\alpha/{\rm Fe}]$ are found in KK 84, a companion of NGC 3115. Other chemical abundances indicate potentially interesting differences between globular clusters in dwarf and more massive galaxies and, if confirmed, would facilitate the quantification of the accreted mass in rich GC systems of massive early-type galaxies.

We thank the referee for a constructive report that helped to improve the paper. T. H. P. gratefully acknowledges support in form of a Plaskett Fellowship at the Herzberg Institute of Astrophysics. This research was supported by the AAS Small Research Grants program. M. E. S. thanks D. I. Makarov for his help with programming in Matlab. We are grateful to Ricardo Schiavon for providing his spectroscopic Milky Way GC data in electronic form. This work is based on observations made with ESO Telescopes at the Paranal Observatory under program ID P76.A-0137 and P76.B-0137.

APPENDIX A

SURFACE BRIGHTNESS PROFILES

Fundamental structural parameters of galaxies determined from their surface brightness (SB) profiles provide valuable information about processes of galaxy formation (e.g., Kormendy 1977; Dekel & Silk 1986). In Tables 1 and 8 we show fundamental photometric parameters obtained for our sample galaxies using our SB profiles. The B and I SB profiles and the corresponding $B - I$ distributions are presented in Figure 9. The errors of SB profile determination depend primarily on the accuracy of the background estimates and the position of the galactic center. The background estimates are relatively uncertain in cases where bright stars are projected on top of the

TABLE 8
FUNDAMENTAL PARAMETERS OF OUR SAMPLE DWARF GALAXIES DERIVED FROM THE SURFACE PHOTOMETRY ON THE VLT/FORS2 IMAGES

Galaxy (1)	$\mu_0(B)$ (2)	$\mu_0(I)$ (3)	$R_e(B)$ (arcsec) (4)	n (5)	R_c (arsec) (6)	R_t (arcsec) (7)
KK 221	26.00 ± 0.20	24.20 ± 0.20	32.3 ± 0.5	0.40 ± 0.20	78 ± 19	85 ± 9
KK 211	24.51 ± 0.12	22.60 ± 0.15	24.1 ± 0.1	0.85 ± 0.15	24 ± 1	89 ± 1
KK 084	24.04 ± 0.07	22.40 ± 0.07	19.4 ± 0.4	0.79 ± 0.01	17 ± 1	75 ± 1
U3755	22.01 ± 0.05	20.98 ± 0.10	22.6 ± 0.1	0.85 ± 0.05	...	...
E490−17	22.45 ± 0.20	21.29 ± 0.05	26.4 ± 1.2	0.76 ± 0.04	...	...

NOTES.—Columns contain the following data: (1) galaxy name; (2) central surface brightness in B band with the corresponding error (a mean value between the corresponding best-fitting parameters of Sersic and King profiles); (3) and (4) best-fitting parameters of the Sersic profile, effective radius and degree with corresponding errors; (5) and (6) the King law approximation parameters, core radius, and effective radius with corresponding errors.

SB profile. That is why our surface photometry results should be taken as rough estimates for this extremely low surface brightness dwarf galaxy KK 221. The choice of a center is complicated for dwarf irregular galaxies with multiple, bright star-forming regions. Given all uncertainties we estimate typical error of the integrated visual magnitude of the order of ∼0.2 mag. The errors of the SB profiles are oveplotted in the distributions of colors in Figure 9.

The solid lines overplotted on the SB profiles show the Sérsic law approximation. The Sérsic model (Sérsic 1968) describes SB profiles of the form

$$I(r) = I_0 \exp\left[-\nu_n (r/r_e)^n\right],$$

where $I(r)$ is the SB (in intensity) at radius r, I_0 is the central surface brightness, r_e is the effective half-intensity radius, $\nu_n \simeq 2n - 1/3 + 4/(405n) + 46/(25515n^2)$, and n is the dimensionless shape parameter that determines the curvature of the profile. For $1/n > 1$ the profiles become flat in the central part, while for $1/n < 1$ they are cuspy. The best-fitting parameters of the Sérsic profile are presented in Table 8. It should be noted that central bright objects such as GCs or star-forming regions were excluded from the fit.

Table 9 summarizes the literature data on the fundamental photometric parameters of our sample galaxies. One can see, that in general our photometric results agree fairly well with the literature data. However, the shape parameter n determined by Jerjen et al. (2000) for KK 211 implies a flatter profile than ours. The color profile is irregular for our sample dIrrs and for KK 221, for which the sky subtraction is difficult.

The Sérsic index n appears to be similar for all our sample dwarf galaxies, except KK 221, which may be tidally disrupted. The SB profile for KK 221 is 2 times flatter than for the other sample galaxies. Similarity of fundamental parameters for rotating and nonrotating dwarf galaxies of different morphological type and situated in different environments may indicate that the internal structure of such faint galaxies is primarily defined by their mass.

APPENDIX B

MASS ESTIMATE FOR KK 221

To derive the mass of KK 221 we use the mass estimator for tracer populations (Evans et al. 2003):

$$M_{\rm press} = \frac{C}{GN} \sum_i (v_{i,\rm los} - \langle v \rangle)^2 R_i, \tag{B1}$$

where

$$C = \frac{16(\gamma - 2\beta)}{\pi(4 - 3\beta)} \frac{4 - \gamma}{3 - \gamma} \frac{1 - (r_{\rm in}/r_{\rm out})^{3-\gamma}}{1 - (r_{\rm in}/r_{\rm out})^{4-\gamma}}. \tag{B2}$$

TABLE 9
FUNDAMENTAL PHOTOMETRIC PARAMETERS FOR OUR SAMPLE GALAXIES FROM LITERATURE SOURCES

Galaxy	B	Color	$R_e(B)$	$\mu_0(B)$	h (arcsec)	Reference
KK 211	16.32	1.56	21.1	24.48	$1.72^{(1/n)}$	Jerjen et al. (2000)
KK 84	16.16	1.38	17.99	23.19	10.59	Parodi et al. (2002)
U3755	14.07	0.55	...	21.64	12.62	Makarova (1999)
E490−017	13.67	0.83	22.83	21.30	13.28	Parodi et al. (2002)

NOTES.—Columns contain the following data: (1) galaxy; (2) total B magnitude; (3) color ($B - R$, except fo for UGC 3755, for which $B - V$ is given); (4) effective radius; (5) central surface brightness; (6) exponential scale length (for KK 211 the Sersic profile shape parameter is given); (7) reference.

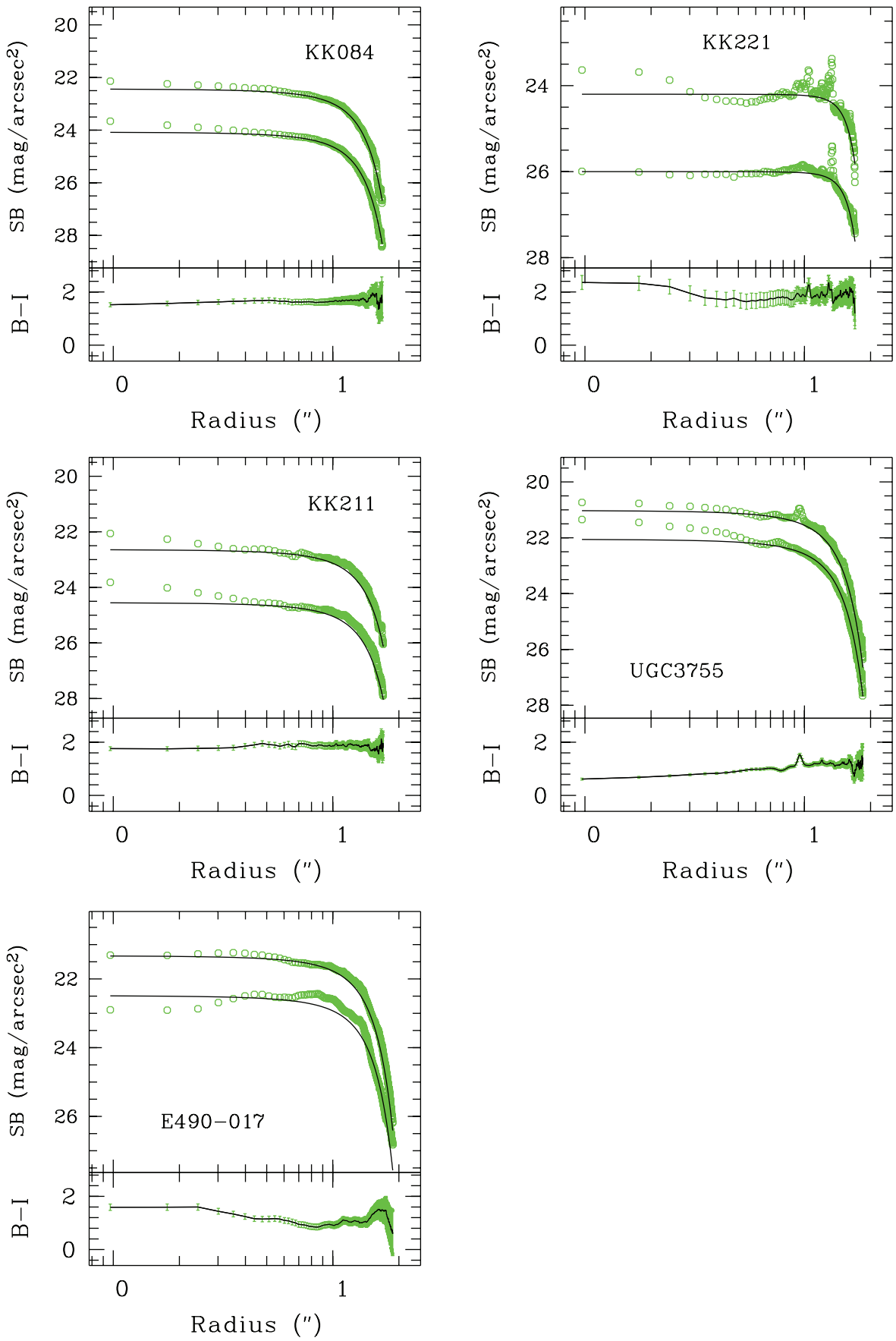

FIG. 9.— Azimuthally averaged surface brightness profiles and $B - I$ color profiles for our sample dwarf galaxies. In all panels, the upper surface brightness curve belongs to the B-band measurement.

TABLE 10

GLOBULAR CLUSTER INDICES (FIRST LINE) CORRECTED FOR ZERO POINTS OF TRANSFORMATION TO THE STANDARD LICK SYSTEM AND ERRORS (±) DETERMINED FROM BOOTSTRAPPING OF THE OBJECT SPECTRUM (SECOND LINE)

ID	S/N[a]	$H\delta_A$ (Å)	$H\gamma_A$ (Å)	$H\delta_F$ (Å)	$H\gamma_F$ (Å)	CN_1 (mag)	CN_2 (mag)	Ca4227 (Å)	G4300 (Å)	Fe4383 (Å)	Ca4455 (Å)	Fe4531 (Å)	Fe4668 (Å)	$H\beta$ (Å)	Fe5015 (Å)	Mg1 (mag)	Mg2 (mag)	Mg *b* (Å)	Fe5270 (Å)	Fe5335 (Å)	Fe5406| (Å)
KK 211																					
149.....	40	4.19	1.41	2.98	2.69	−0.1272	−0.0867	0.12	1.34	1.93	0.07	1.19	1.28	3.33	2.56	−0.0142	0.0538	1.05	0.93	1.03	0.21
		0.22	0.23	0.23	0.23	0.0021	0.0031	0.11	0.12	0.14	0.14	0.15	0.18	0.18	0.19	0.0050	0.0050	0.20	0.20	0.20	0.21
KK 221																					
966.....	85	2.42	0.67	2.21	2.25	−0.1319	−0.1006	0.61	1.44	1.05	0.39	1.79	−0.12	1.97	1.93	0.0065	0.0566	0.85	0.86	0.48	0.14
		0.09	0.09	0.09	0.10	0.0007	0.0011	0.04	0.04	0.05	0.05	0.06	0.07	0.07	0.08	0.0020	0.0020	0.08	0.08	0.08	0.09
24n.....	35	3.16	1.46	3.30	2.43	−0.0963	−0.1251	0.88	1.60	−0.73	0.27	1.20	2.29	2.49	1.74	0.0119	0.0581	0.66	1.36	0.20	−0.18
		0.24	0.24	0.25	0.25	0.0019	0.0029	0.11	0.12	0.15	0.15	0.17	0.20	0.20	0.21	0.0054	0.0055	0.22	0.22	0.22	0.22
KK 084																					
705.....	31	1.10	−0.90	2.00	1.97	−0.1074	−0.0493	0.68	3.12	0.57	0.83	1.42	2.71	2.15	1.35	0.0333	0.1000	1.36	0.62	−0.26	1.02
		0.21	0.21	0.22	0.22	0.0018	0.0027	0.09	0.10	0.13	0.13	0.14	0.16	0.16	0.18	0.0047	0.0047	0.18	0.19	0.19	0.19
830.....	47	3.82	0.96	2.81	2.06	−0.1075	−0.0693	0.60	1.93	1.38	0.80	0.01	−0.58	1.90	1.83	0.0182	0.0536	0.80	1.15	0.35	−0.21
		0.07	0.07	0.07	0.07	0.0006	0.0009	0.03	0.03	0.04	0.04	0.05	0.06	0.06	0.06	0.0016	0.0016	0.06	0.06	0.07	0.07
666.....	24	−2.06	−6.21	0.07	−1.40	0.0343	0.0736	1.93	6.98	4.65	2.25	3.02	6.38	1.56	2.95	0.0643	0.1977	2.58	1.73	1.61	1.28
		0.28	0.29	0.30	0.30	0.0025	0.0041	0.13	0.15	0.18	0.18	0.19	0.22	0.22	0.24	0.0072	0.0073	0.24	0.25	0.25	0.25
36n.....	23	−1.23	−4.00	−0.45	−0.23	−0.0374	0.0087	0.45	2.35	−0.08	0.62	2.22	1.16	1.23	5.91	0.0592	0.1589	2.60	2.58	1.97	−0.21
		0.19	0.19	0.20	0.20	0.0018	0.0026	0.08	0.09	0.12	0.12	0.13	0.15	0.15	0.16	0.0044	0.0044	0.17	0.17	0.17	0.00
U3755																					
652.....	42	3.76	−2.35	3.15	0.83	−0.0868	−0.0420	0.73	2.30	3.12	0.85	1.85	1.17	1.83	1.94	0.0194	0.0665	1.16	1.02	0.68	0.24
		0.12	0.12	0.12	0.12	0.0011	0.0017	0.06	0.06	0.08	0.08	0.08	0.09	0.10	0.10	0.0028	0.0029	0.11	0.11	0.11	0.11
914.....	23	6.72	4.57	4.47	4.03	−0.1930	−0.1193	0.38	0.35	−1.28	0.83	0.26	−1.05	4.31	0.08	−0.0001	0.0661	1.47	1.28	0.66	0.36
		0.18	0.18	0.18	0.18	0.0012	0.0017	0.06	0.07	0.09	0.09	0.10	0.13	0.14	0.15	0.0036	0.0037	0.16	0.17	0.17	0.17
1182.....	49	8.48	6.78	6.49	5.38	−0.2120	−0.1678	0.59	−1.98	−0.41	−0.17	1.13	−0.34	5.89	2.17	−0.0153	0.0232	0.25	0.86	−0.30	−0.27
		0.08	0.08	0.08	0.08	0.0006	0.0009	0.03	0.04	0.04	0.05	0.05	0.06	0.07	0.07	0.0017	0.0017	0.07	0.07	0.08	0.08
1257.....	25	3.26	1.05	2.84	2.30	−0.0894	−0.0769	0.89	3.08	−0.10	0.51	0.73	0.23	2.78	3.00	0.0197	0.0667	1.25	2.26	1.11	1.02
		0.20	0.20	0.20	0.21	0.0019	0.0026	0.09	0.10	0.12	0.12	0.13	0.16	0.16	0.17	0.0045	0.0046	0.18	0.18	0.18	0.18
2123.....	31	4.94	2.87	3.41	3.16	−0.1327	−0.1067	0.81	−0.72	1.50	1.31	2.31	−0.06	2.59	0.25	−0.0020	0.0167	0.24	0.88	0.89	0.26
		0.14	0.14	0.14	0.14	0.0010	0.0014	0.05	0.06	0.07	0.07	0.08	0.10	0.10	0.11	0.0028	0.0029	0.12	0.13	0.13	0.13
2363.....	38	9.32	6.76	6.03	6.02	−0.1690	−0.1133	0.60	−1.07	0.93	0.31	1.66	0.04	5.43	1.20	0.0091	0.0330	0.47	0.90	0.66	−0.52
		0.10	0.12	0.11	0.11	0.0007	0.0012	0.04	0.05	0.06	0.06	0.07	0.08	0.08	0.09	0.0023	0.0023	0.10	0.10	0.10	0.10
2459.....	44	7.58	7.39	5.88	5.54	−0.2170	−0.1784	0.57	−1.55	−1.01	0.30	1.37	−0.38	4.92	1.18	0.0048	0.0442	1.03	1.27	0.63	−0.13
		0.10	0.10	0.10	0.10	0.0007	0.0011	0.04	0.04	0.05	0.06	0.06	0.08	0.08	0.08	0.0022	0.0022	0.09	0.10	0.10	0.10
E490−17																					
2035.....	13	4.63	4.94	4.84	4.94	−0.1082	−0.0853	1.18	0.26	0.21	0.33	0.11	−1.76	4.50	0.64	0.0084	0.0426	0.47	0.63	1.61	0.38
		0.55	0.56	0.56	0.57	0.0035	0.0055	0.20	0.21	0.26	0.27	0.30	0.40	0.41	0.45	0.0111	0.0113	0.49	0.51	0.52	0.53
1861.....	17	2.60	1.10	2.93	1.90	−0.0666	−0.0611	0.32	1.06	−0.40	1.25	0.07	−0.38	1.42	1.17	0.0224	0.0413	1.10	0.34	0.16	0.36
		0.47	0.48	0.49	0.49	0.0038	0.0055	0.19	0.22	0.27	0.27	0.31	0.37	0.37	0.40	0.0105	0.0106	0.42	0.43	0.44	0.44

[a] Approximate S/N ratios per Å measured at 5000 Å.

Here, $\langle v\rangle$ is the system's mean radial velocity and β the anisotropy parameter $1 - \sigma_t^2/\sigma_r^2$, which is unity for purely radial orbits and $-\infty$ for a system with solely tangential orbits (Binney 1981).

Using the power-law rule $\gamma 1 + d\log\Sigma/d\log R$ (Gebhardt et al. 1996) to derive the three-dimensional density profile of the GC population, we obtain $\gamma = 1.4$ from the Sersic index n of KK 221 SB distribution (see Table 1), and $M_{\rm press} \approx 3\times10^8\ M_\odot$. We use here the anisotropy parameter $\beta = 0.5$ for randomly oriented orbits, and radii of orbits of the nearest and most distant GC $r_{\rm in} = 0.9$ kpc and $r_{\rm out} = 1.8$ kpc (Sharina et al. 2005), correspondingly. The statistically unbiased estimate of the mass value is $M^c_{\rm press} = M_{\rm press}[1 - (2\sigma_v^2)/3s_v^2]$, where σ_v is the rms error of the radial velocity measurements, and s_v is the rms velocity of GCs relative to the mean velocity of GC system, $s_v^2 = (1/k)\sum(v_k - \langle v\rangle)^2$ with a number of GCs equal k (Karachentsev 1999). $M^c_{\rm press} = 0.2M_{\rm press}$ in our case. So, we obtain the statistically unbiased estimate of the mass for KK 221 $M^c_{\rm press} \sim 6\cdot10^7\ M_\odot$, and the corresponding mass-to-light ratio $M/L_v \approx 15$. Corrected for the effect of radial velocity anisotropy (§ 3.2), the mass-to-light ratio M/L_v appears to be $\sim 9M/L_{v,\odot}$. The expected uncertainty of the total mass estimate is ~50% taking into account the small number of GCs. In our case, where the number of GCs is six, the error of the velocity dispersion measurement is ~33% of the value of the velocity dispersion itself.

APPENDIX C

LICK INDEX MEASUREMENTS

We provide the calibrated Lick index measurements of all confirmed GCs in Table 10.

REFERENCES

Arimoto, N., & Yoshii, Y. 1987, A&A, 173, 23
Barmby, P., Huchra, J. P., Brodie, J. P., Forbes, D. A., Schroder, L. L., & Grillmair, C. J. 2000, AJ, 119, 727
Beasley, M. A., Brodie, J. P., Strader, J., Forbes, D. A., Proctor, R. N., Barmby, P., & Huchra, J. P. 2005, AJ, 129, 1412
Beasley, M. A., Hoyle, F., & Sharples, R. M. 2002, MNRAS, 336, 168
Beasley, M. A., Strader, J., Brodie, J.P, Cenarro, A. J., & Geha, M. 2006, AJ, 131, 814
Benson, A. J., Sugiyama, N., Nusser, A., & Lacey, C. G. 2006, MNRAS, 369, 1055
Bicay, M. D., & Giovanelli, R. 1986, AJ, 91, 732
Binggeli, B., Sandage, A., & Tammann, G. A. 1985, AJ, 90, 1681
Binney, J. 1981, Structure and Evolution of Normal Galaxies, ed. D. Lynden-Bell & S. M. Fall (Cambridge: Cambridge: Univ. Press)
Bruzual, G., & Charlot, S. 2003, MNRAS, 344, 1000
Burstein, D., et al. 2004, ApJ, 614, 158
Cenarro, A. J., Sánchez-Blázquez, P., Cardiel, N., & Gorgas, J. 2004, ApJ, 614, L101
Chandar, R., Fall, S. M., & Whitmore, B. C. 2006, ApJ, 650, L111
Clemens, M. S., Bressan, A., Nikolic, B., Alexander, P., Annibali, F., & Rampazzo, R. 2006, MNRAS, 370, 702
Conselice, C. J. 2006, ApJ, 639, 120
Côté, P., Marzke, R. O., & West, M. J. 1998, ApJ, 501, 554
Côté, P., West, M. J., & Marzke, R. O. 2002, ApJ, 567, 853
Côté, P., et al. 2006, ApJS, 165, 57
Dekel, A., & Silk, J. 1986, ApJ, 303, 39
Dekel, A., & Woo, J. 2003, MNRAS, 344, 1131
De Lucia, G., Springel, V., White, S. D. M., Croton, D., & Kauffmann, G. 2006, MNRAS, 366, 499
Di Criscienzo, M., Caputo, F., Marconi, M., & Musella, I. 2006, MNRAS, 365, 1357
Durrel, P., Harris, W., Geisler, D., & Pudritz 1996, AJ, 112, 972
Ellis, R. S. 2007, in First Light in the Universe, ed. A. Loeb, A. Ferrara, & R. S. Ellis (Berlin: Springer), 259
Elmegreen, B. G., & Shadmehri, M. 2003, MNRAS, 338, 817
Evans, N. W., Wilkinson, M. I., Perrett, K. M., & Bridges, T. J. 2003, ApJ, 583, 752
Fall, S. M., & Zhang, Q. 2001, ApJ, 561, 751
Forte, J. C., Martinez, R. E., & Muzzio, J. C. 1982, AJ, 87, 1465
Fouqué, P., Solanes, J. M., Sanchis, T., & Balkowski, C. 2001, A&A, 375, 770
Freeman, K., & Bland-Hawthorn, J. 2002, ARA&A, 40, 487
Gebhardt et al. 1996, AJ, 112, 105
Geisler, D., Wallerstein, G., Smith, V. V., & Casetti-Dinescu, D. I. 2007, PASP, 119, 939
Georgiev, I. Y., Hilker, M., Puzia, T. H., Chanamé, J., Mieske, S., Goudfrooij, P., Reisenegger, A., & Infante, L. 2006, A&A, 452, 141
Gnedin, O. Y. 2003, ApJ, 589, 752
Grebel, E. K. 1999, IAU Symp. 192, The Stellar Content of Local Group Galaxies, ed. P. Whitelock & R. Cannon (ASP Conf. Ser. 17; San Francisco: ASP), 447
———. 2006, preprint (astro-ph/0605564)
Grebel, E. K., Gallagher, J. S., III, & Harbeck, D. 2003, AJ, 125, 1926
Greggio, L. 2005, A&A, 441, 1055
Harris, W. E. 1991, ARA&A, 29, 543
Harris, W. E., & van den Bergh, S. 1981, AJ, 86, 1627
Hilker, M., Infante, L., & Richtler, T. 1999, A&AS, 138, 55
Holtzman, J. A., Afonso, C., & Dolphin, A. 2006, ApJS, 166, 534
Hunter, D. A., & Gallagher, J. S. 1985, ApJS, 58, 533
Impey, C., & Bothun, G. 1997, ARA&A, 35, 267
James, P. A., Shane,N. S., Knapen, J. H., Etherton, J., & Percival, S. M. 2005, A&A, 429, 851
Jerjen, H., Binggeli, B., & Freeman, K. C. 2000, AJ, 119, 593
Jordán, A., et al. 2007, ApJS, 171, 101
Karachentsev, I. D. 1999, Astron. Lett., 25, 318
Karachentsev, I. D., Karachentseva, V. E., Huchtmeier, W. K., & Makarov, D. I. 2004, AJ, 127, 2031
Karachentsev, I. D., & Kashibadze, O. G. 2005, preprint (astro-ph/0509207)
Karachentseva, V. E., Karachentsev, I. D., & Boerngen, F. 1985, A&AS, 60, 213
Kashikawa, N., et al. 2006, ApJ, 648, 7
Kauffmann, G. 1996, MNRAS, 281, 487
Kerber, L. O., Santiago, B. X., & Brocato, E. 2007, A&A, 462, 139
Kormendy, J. 1977, ApJ, 218, 333
Kumai, Y., Hashi, Y., & Fujimoto, M. 1993, ApJ, 416, 576
Kuntschner, H., Ziegler, B. L., Sharples, R. M., Worthey, G., & Fricke, K. J. 2002, A&A, 395, 761
Lanfranchi, G. A., & Matteucci, F. 2003, MNRAS, 345, 71
Li, Y., & Burstein, D. 2003, ApJ, 598, L103
Lisker, T., Grebel, E. K., Binggeli, B., & Glatt, K. 2007, ApJ, 660, 1186
Makarova, L. N. 1999, A&AS, 139, 491
Matteucci, F. 1994, A&A, 288, 57
McLaughlin, D. E. 1999, AJ, 117, 2398
McLaughlin, D. E., King, A. R., & Nayakshin, S. 2006, ApJ, 650, L37
Miller, B. W. 2006, preprint (astro-ph/0606062)
Miller, B. W., Lotz, J. M., Ferguson, H. C., Stiavelli, M., & Whitmore, B. C. 1998, ApJ, 508, L133
Muzzio, J. C. 1987, PASP, 99, 245
Nayakshin, S., Cuadra, J., & Springel, V. 2007, MNRAS, 379, 21
Nayakshin, S., Dehnen, W., Cuadra, J., & Genzel, R. 2006, MNRAS, 366, 1410
Nomoto, K., Iwamoto, K., Nakasato, N., Thielemann, F.-K., Brachwitz, F., Tsujimoto, T., Kubo, Y., & Kishimoto, N. 1997, Nucl. Phys. A, 621, 467
Norris, M. A., Sharples, R. M., & Kuntschner, H. 2006, MNRAS, 367, 815
Osterbrock, D. E., Fulbright, J. P., Martel, A. R., Keane, M. J., Trager, S. C., & Basri, G. 1996, PASP, 108, 277
Osterbrock, D. E., Waters, R. T., Barlow, T. A., Slanger, T. G., & Cosby, P. C. 2000, PASP, 112, 733
Parodi, B. R., Barazza, F. D., B. & Binggeli, B. 2002, A&A, 388, 29
Peebles, P. J. E. 2002, in ASP Conf. Ser. 283, A New Era in Cosmology, ed. N. Metcalfe & T. Shank (San Francisco: ASP), 351
Peebles, P. J. E., & Dicke, R. H. 1968, ApJ, 154, 891
Pipino, A., Puzia, T. H., & Matteucci, F. 2007, ApJ, 665, 295
Pritzl, B. J., Venn, K. A., & Irwin, M. 2005, AJ, 130, 2140
Prochaska, L. C., Rose, J. A., & Schiavon, R. P. 2005, AJ, 130, 2666
Puzia, T. H., Kissler-Patig, M., Brodie, J. P., & Schroder, L. L. 2000, AJ, 120, 777
Puzia, T. H., Kissler-Patig, M., & Goudfrooij, P. 2006, ApJ, 648, 383
Puzia, T. H., Perrett, K. M., & Bridges, T. J. 2005a, A&A, 434, 909
Puzia, T. H., Saglia, R. P., Kissler-Patig, M., Maraston, C., Greggio, L., Renzini, A., & Ortolani, S. 2002, A&A, 395, 45

Puzia, T. H., et al. 2004, A&A, 415, 123 (P04)
———. 2005b, A&A, 439, 997
Recchi, S., & Danziger, I. J. 2005, A&A, 436, 145
Rejkuba, M., Greggio, L., Harris, W. E., Harris, G. L. H., & Peng, E. W. 2005, ApJ, 631, 262
Renzini, A. 2006, ARA&A, 44, 141
Richtler, T. 1995, Rev. Mod. Astron., 8, 163
Robin, A. C., Reylé, C., Derrière, S., & Picaud, S. 2003, A&A, 409, 523
Sandage, A., Binggeli, B., & Tammann, G. A. 1985, AJ, 90, 1759
Schiavon, R. P., Rose, J. A., Courteau, S., & MacArthur, L. A. 2005, ApJS, 160, 163
Schlegel, D. J., Finkbeiner, D. P., & Davis, M. 1998, ApJ, 500, 525
Sersic, L.-J. 1968, Atlas de Galaxias Australes (Cordova: Obs. Astron)
Sharina, M. E., Afanasiev, V. L., & Puzia, T. H. 2006, MNRAS, 372, 1259
Sharina, M. E., Puzia, T. H., & Makarov, D. I. 2005, A&A, 442, 85 (SPM05)
Sharina, M. E., Sil'chenko, O. K., & Burenkov, A. N. 2003, A&A, 397, 831
Spergel, D. N., et al. 2003, ApJS, 148, 175
Stetson, P. B. 1987, PASP, 99, 191
Strader, J., Brodie, J. P., Forbes, D. A., Beasley, M. A., & Huchra, J. P. 2003a, AJ, 125, 1291
Strader, J., Brodie, J. P., & Huchra, J. P. 2003b, MNRAS, 339, 707
Thomas, D., Maraston, C., & Bender, R. 2003, MNRAS, 339, 897
Thomas, D., Maraston, C., Bender, R., & Mendes de Oliveira, C. 2005, ApJ, 621, 673
Thomas, D., Maraston, C., & Korn, A. 2004, MNRAS, 351, L19
Tonry, J., & Davis, M. 1979, AJ, 84, 1511
Treu, T., et al. 2005, ApJ, 633, 174
Tripicco, M. J., & Bell, R. A. 1995, AJ, 110, 3035
Tully, R. B., Somerville, R. S., Trentham, N., & Verheijen, M. A. W. 2002, ApJ, 569, 573
Tully, R. B., et al. 2006, AJ, 132, 729
van den Bergh, S. 2006, The Local Group as an Astrophysical Laboratory, ed. M. Livio & T. M. Brown (Baltimore: STScI), 1
———. 2007, AJ, 134, 344
Villanova, S., et al. 2007, ApJ, 663, 296
West, M. J. 1993, MNRAS, 265, 755
Whitmore, B. C., Chandar, R., & Fall, S. M. 2007, AJ, 133, 1067
Woosley, S. E., Heger, A., & Weaver, T. A. 2002, Rev. Mod. Phys., 74, 1015
Worthey, G. 1994, ApJS, 95, 107
Worthey, G., & Ottaviani, D. L. 1997, ApJS, 111, 377